

1 **Endogenous *Syngap1* Alpha Splice Forms Promote Cognitive  
2 Function and Seizure Protection**

3 Murat Kilinc<sup>1,2</sup>, Vineet Arora<sup>2</sup>, Thomas K. Creson<sup>2</sup>, Camilo Rojas<sup>2</sup>, Aliza A. Le<sup>4</sup>, Julie  
4 Lauterborn<sup>4</sup>, Brent Wilkinson<sup>5</sup>, Nicolas Hartel<sup>6</sup>, Nicholas Graham<sup>6</sup>, Adrian Reich<sup>3</sup>,  
5 Gemma Gou<sup>7,8</sup>, Yoichi Araki<sup>9</sup>, Àlex Bayés<sup>7,8</sup>, Marcelo P. Coba<sup>5</sup>, Gary Lynch<sup>4</sup>, Courtney  
6 A. Miller<sup>1,2</sup>, Gavin Rumbaugh<sup>1,2#</sup>

7  
8  
9 <sup>1</sup>*Graduate School of Chemical and Biological Sciences, <sup>2</sup>Departments of Neuroscience and  
10 Molecular Medicine, <sup>3</sup>Bioinformatics and Statistics Core, The Scripps Research Institute, The  
11 Scripps Research Institute, Jupiter, FL, USA*

12 <sup>4</sup>*Department of Anatomy and Neurobiology, The University of California, Irvine, CA, USA*

13 <sup>5</sup>*Zilkha Neurogenetic Institute, Keck School of Medicine, University of Southern California, Los  
14 Angeles, CA, USA.*

15 <sup>6</sup>*Mork Family Department of Chemical Engineering and Materials Science, University of  
16 Southern California, Los Angeles, California*

17 <sup>7</sup>*Molecular Physiology of the Synapse Laboratory, Biomedical Research Institute Sant Pau (IIB  
18 Sant Pau), Barcelona, Spain.*

19 <sup>8</sup>*Universitat Autònoma de Barcelona, 08193 Bellaterra (Cerdanyola del Vallès), Spain*

20 <sup>9</sup>*Department of Neuroscience, Johns Hopkins University School of Medicine, Baltimore,  
21 MD 21205, USA.*

22  
23  
24 #Correspondence and Lead Contact: Gavin Rumbaugh, Ph.D.  
25 The Scripps Research Institute  
26 120 Scripps Way, #3B3  
27 Jupiter, FL 33458  
28 561-228-3461  
29 [gavin@scripps.edu](mailto:gavin@scripps.edu)

32 **Summary**

33 Loss-of-function variants in *SYNAGP1* cause a developmental encephalopathy defined by  
34 cognitive impairment, autistic features, and epilepsy. *SYNGAP1* splicing leads to expression of  
35 distinct functional protein isoforms. Splicing imparts multiple cellular functions of SynGAP  
36 proteins through coding of distinct C-terminal motifs. However, it remains unknown how these  
37 different splice sequences function *in vivo* to regulate neuronal function and behavior. Reduced  
38 expression of SynGAP- $\alpha$ 1/2 C-terminal splice variants in mice caused severe phenotypes,  
39 including reduced survival, impaired learning, and reduced seizure latency. In contrast,  
40 upregulation of  $\alpha$ 1/2 expression improved learning and increased seizure latency. Mice  
41 expressing  $\alpha$ 1-specific mutations, which disrupted SynGAP cellular functions without altering  
42 protein expression, promoted seizure, disrupted synapse plasticity, and impaired learning.  
43 These findings demonstrate that endogenous SynGAP isoforms with  $\alpha$ 1/2 spliced sequences  
44 promote cognitive function and impart seizure protection. Regulation of SynGAP- $\alpha$  expression  
45 or function may be a viable therapeutic strategy to broadly improve cognitive function and  
46 mitigate seizure.

47

48 **Key Words:** *Syngap1*, SynGAP, Synapse, Plasticity, PSD95, PDZ domain, Long-term  
49 potentiation, Intellectual disability, Autism spectrum disorder, Epilepsy, Learning, Behavior

50 **Introduction**

51 Pathogenic variation in *SYNGAP1*, the gene encoding SynGAP proteins, is a leading cause of  
52 sporadic neurodevelopmental disorders (NDDs) defined by impaired cognitive function, seizure,  
53 autistic features, and challenging behaviors [1-8]. *De novo* loss-of-function variants leading to  
54 *SYNGAP1* haploinsufficiency cause a genetically-defined developmental encephalopathy (IDC-  
55 10 code: F78.A1) that overlaps substantially with diagnoses of generalized epilepsy, global  
56 developmental delay, intellectual disability, and autism [4-6, 9, 10]. *SYNGAP1* is completely  
57 intolerant of loss-of-function (LOF) variants [11]. Thus, the presence of a clear LOF variant in a  
58 patient will lead to the diagnosis of a *SYNGAP1*-mediated developmental encephalopathy. The  
59 range of neuropsychiatric disorders causally linked to *SYNGAP1* pathogenicity, combined with  
60 the complete penetrance of LOF variants in humans, demonstrate the crucial role that this gene  
61 plays in the development and function of neural circuits that promote cognitive abilities,  
62 behavioral adaptations, and balanced excitability.

63  
64 SynGAP proteins have diverse cellular functions [11-13]. The best characterized of these is the  
65 regulation of excitatory synapse structure and function located on forebrain glutamatergic  
66 projection neurons. In these synapses, SynGAP is predominately localized within the  
67 postsynaptic density (PSD), where it exists in protein complexes with synapse-associated-  
68 protein (SAP) family proteins [14, 15]. Within these complexes, SynGAP proteins regulate  
69 signaling through NMDARs, where they constrain the activity of various small GTPases through  
70 non-canonical activity of a RasGAP domain [12, 13]. This regulation of GTPase activity is  
71 required for excitatory synapse plasticity [16, 17]. Reduced expression of SynGAP in both  
72 human and rodent neurons causes enhanced excitatory synapse function during early brain  
73 development and is a process thought to impair cognitive functioning [11, 18, 19]. SynGAP also  
74 regulates dendritic arborization. Reduced SynGAP protein expression impairs the development  
75 of dendritic arborization in neurons derived from both rodent and human tissues [11, 20, 21],  
76 which disrupts the function and excitability of neural networks from both species. While reduced  
77 SynGAP expression enhances postsynaptic function regardless of glutamatergic projection  
78 neuron subtype, this same perturbation has an unpredictable impact on dendritic arborization,  
79 with some neurons undergoing precocious dendritic morphogenesis [11, 20], while others  
80 displaying stunted morphogenesis [21]. This is an example of pleiotropy, where *Syngap1* gene  
81 products have unique functions depending on the neuronal subtype, or possibly within distinct  
82 subcellular compartments of the same type of neuron.

83  
84 How SynGAP performs diverse cellular functions remains unclear. One potential mechanism is  
85 through alternative splicing. Indeed, the last three exons of *Syngap1* undergo alternative  
86 splicing[22-24], which results in four distinct C-termini ( $\alpha 1$ ,  $\alpha 2$ ,  $\beta$ ,  $\gamma$ ). These SynGAP C-terminal  
87 protein isoforms are expressed in both rodents and humans, and they are spatially and  
88 temporally regulated across mammalian brain development [22, 23]. Moreover, protein motifs  
89 present within these differentially expressed C-termini impart SynGAP with distinct cellular  
90 functions, with  $\alpha$ -derived motifs shown to regulate post-synapse structure and function[25, 26],  
91 while the  $\beta$ -derived sequences linked to *in vitro* dendritic morphogenesis [22]. *Syngap1*  
92 heterozygous mice, which model the genetic impact of *SYNGAP1* haploinsufficiency in humans,  
93 express a robust endophenotype characterized by increased horizontal activity, poor  
94 learning/memory, and seizure [12, 16, 18, 27, 28]. Currently, it remains unknown to what extent  
95 endogenous *in vivo* expression of alternatively spliced isoforms contribute to systems-level  
96 endophenotypes expressed in animal models.

97  
98 **Results**

99 The last three exons of *Syngap1* undergo alternative splicing (**Fig. 1A**), which results in four  
100 distinct C-termini (**Fig. 1B**). Exon 19 is spliced into two reading frames (e19b/e19a) (**Fig. 1C**).

101 Because e19b lacks a stop codon, coding sequences from e20 and e21 are also included in  
102 mature transcripts. This leads to expression of  $\alpha$ 1,  $\alpha$ 2, or  $\gamma$  C-terminal isoforms (**Fig. 1C-D**).  $\gamma$   
103 isoforms arise from inclusion e20, while  $\alpha$ 1 and  $\alpha$ 2 arise from the absence of e20, but inclusion  
104 of e21. e21 itself has two reading frames, with one leading to expression of  $\alpha$ 1 while the other  
105 codes for  $\alpha$ 2 (**Fig. 1E**). SynGAP- $\beta$  arises from splicing of e19 into the “a” reading frame, which  
106 contains an internal stop codon (**Fig. 1C**). To address how expression or function of isoforms  
107 contribute to cognitive function, behavior, and seizure latency, we created three distinct mouse  
108 lines, each with targeted modifications within the final three exons of the *Syngap1* gene. Each  
109 line expressed a unique signature with respect to C-terminal SynGAP protein variant expression  
110 or function. For example, in the *Syngap1*<sup>td/td</sup> line,  $\alpha$  isoform expression was disrupted while  $\beta$   
111 forms were upregulated (**Fig. 1F-G**). In contrast, *Syngap1* <sup>$\beta/\beta^*$</sup>  mice were opposite with respect to  
112 expression of  $\alpha$  and  $\beta$  isoforms, with the former upregulated and the latter disrupted (**Fig. 1H**).  
113 Finally, the *Syngap1*<sup>PBM/PBM</sup> line, which expressed point mutations that selectively disrupted an  
114 essential function of SynGAP- $\alpha$ 1 (**Fig. 1I**), was useful for determining to what extent phenotypes  
115 in the other two lines may have been driven by upregulated or downregulated isoforms.  
116

117 Reduced  $\alpha$ 1/2 C-Terminal Isoform Expression is Associated with Enhanced Seizure Latency  
118 and Cognitive impairment

119 We previously reported the generation of a *Syngap1* mouse line with an insertion of an IRES-  
120 TDtomato (IRES-TD) cassette within the 3'-UTR to facilitate endogenous reporting of active  
121 *Syngap1* mRNA translation in cells [29]. The cassette was placed within the last *Syngap1* exon  
122 (e21) between the stop codons of  $\alpha$ 1 and  $\alpha$ 2 coding sequences (**Fig. 1E; Fig. 2A**). Our prior  
123 study reported neuronal expression of fluorescent protein and normal total SynGAP (t-SynGAP)  
124 protein expression as measured by antibodies that recognize all splice forms. Due to our  
125 interest in understanding how *in vivo* expression of C-terminal variants impacts brain systems  
126 and behavior, we performed an in-depth characterization of behavioral phenotypes and  
127 SynGAP isoform expression in IRES-TD mice. Heterozygous (*Syngap1*<sup>+/td</sup>) breeding of IRES-TD  
128 animals resulted in offspring of expected mendelian ratios (**Fig. 2B**). However, while all WT  
129 (*Syngap1*<sup>++</sup>) mice survived during the 100-day observation period, significant post-weaning  
130 death occurred in IRES-TD mice, with approximately two-thirds of homozygous mice  
131 (*Syngap1*<sup>td/td</sup>) failing to survive past PND 50 (**Fig. 2B**). It is well established that complete loss of  
132 t-SynGAP protein stemming from homozygous inclusion of null alleles leads to early postnatal  
133 death [27, 30]. However, ~50% t-SynGAP expression, like that occurring in heterozygous KO  
134 mice (*Figure 2 -supplement 1A*), has no impact on survival [27, 30]. Given the unexpectedly  
135 poor survival of *Syngap1*<sup>td/td</sup> animals, we thoroughly examined SynGAP C-terminal isoform  
136 protein expression in this line. At PND21, when all three genotypes are abundant (**Fig. 2B**), t-  
137 SynGAP protein in mouse cortex homogenate was reduced in *Syngap1*<sup>+/td</sup> and *Syngap1*<sup>td/td</sup> mice  
138 compared to WT controls (**Fig. 2C**). Reduced t-SynGAP levels appeared to be largely driven by  
139 near-complete disruption of  $\alpha$ 1/2 protein expression from the targeted allele. Reduced  $\alpha$  isoform  
140 expression coincided with increased protein levels of  $\beta$ -containing C-terminal isoforms. Even  
141 with  $\beta$  compensation, *Syngap1*<sup>td/td</sup> mice expressed only ~50% of t-SynGAP at PND21. Whole  
142 exome sequencing was carried out in each genotype. Differential gene expression (DGE)  
143 analysis revealed only a single mRNA, *Syngap1*, was abnormally expressed (*Supplemental  
144 Table 1*). There was a ~25% reduction in mRNA levels in both *Syngap1*<sup>+/td</sup> and *Syngap1*<sup>td/td</sup> mice  
145 (*Figure 2 -supplement 1B*). While the IRES-TD cassette destabilized a proportion of *Syngap1*  
146 mRNAs, the similarity in mRNA levels from both *Syngap1*<sup>+/td</sup> and *Syngap1*<sup>td/td</sup> samples indicated  
147 that other mechanisms must also contribute to reduced protein expression of  $\alpha$ 1/2 isoforms.  
148 Indeed, a recent study identified 3'UTR-dependent regulation of  $\alpha$  isoform protein expression  
149 [31], suggesting that the IRES-TD cassette is also disrupting translation of these C-terminal  
150 variants. We next addressed expression of SynGAP isoforms in adulthood. In this additional

151 experiment, only *Syngap1<sup>+/+</sup>* and *Syngap1<sup>+/td</sup>* mice were used because of limited survival and  
152 poor health of homozygous mice in the post-weaning period (**Fig. 2B**). The general pattern of  
153 abnormal SynGAP levels persisted into adulthood, with both  $\alpha$  isoforms reduced by ~50%  
154 compared to WT levels, while  $\beta$  isoforms were significantly enhanced (*Figure 2 -supplement*  
155 **1C**). However, the effect on t-SynGAP was less pronounced in older animals and did not rise to  
156 significance. This finding highlights the importance of measuring the expression of individual  
157 isoforms in addition to total levels of SynGAP protein in samples derived from animal or cellular  
158 models.

159  
160 *Syngap1* heterozygous KO mice, which have 50% reduction of t-SynGAP and 50% reduction of  
161 all isoforms (*Figure 2 -supplement 1A*), have normal post-weaning survival rates [27, 30].  
162 However, survival data from *Syngap1<sup>td/td</sup>* mice above, which also expressed a ~50% reduction  
163 of t-SynGAP, but loss of  $\alpha$  isoform expression (**Fig. 2C; Fig. 1G**), suggest that expression of  
164 these isoforms is required for survival.  $\alpha$  isoforms are highly enriched in brain [22], suggesting  
165 that reduced survival stems from altered brain function. Therefore, we next sought to  
166 understand how reduced  $\alpha 1/2$  expression (but in the context of  $\beta$  compensation) impacted  
167 behaviors known to be sensitive to reduced t-SynGAP expression in mice. We obtained minimal  
168 data from adult *Syngap1<sup>td/td</sup>* mice because they exhibit poor health and survival in the post-  
169 weaning period. However, two animals were successfully tested in the open field, and they  
170 exhibited very high levels of horizontal activity (**Fig. 2D**). A more thorough characterization of  
171 behavior was carried out in adult *Syngap1<sup>+/td</sup>* mice, which have significantly reduced  $\alpha$  isoforms,  
172 enhanced  $\beta$  expression, but relatively normal t-SynGAP levels (*Figure 2 -supplement 1A*).  
173 *Syngap1<sup>+/td</sup>* mice exhibited significantly elevated open field activity, seized more quickly in  
174 response to flurothyl, and froze less during remote contextual fear memory recall (**Fig. 2E-G**).  
175 These phenotypes are all present in conventional *Syngap1<sup>+/−</sup>* mice [16, 18, 20, 32], which again  
176 express ~50% reduction of all isoforms (*Figure 2 -supplement 1A*). In contrast, Morris water  
177 maze acquisition, which is also impaired in *Syngap1<sup>+/−</sup>* mice [27, 30], was unchanged in  
178 *Syngap1<sup>+/td</sup>* mice (**Fig. 2H**). Thus, certain behaviors, including horizontal activity, freezing in  
179 response to conditioned fear, and behavioral seizure, are sensitive to reduced levels of  $\alpha$   
180 isoforms, but not necessarily t-SynGAP levels.  
181

### 182 Enhanced $\alpha 1/2$ C-Terminal Isoform Expression is Associated with Seizure Protection and 183 Improved Cognitive Function

184 The results in IRES-TD mice suggested that certain core *Syngap1*-sensitive behavioral  
185 phenotypes are caused, at least in part, by reduced  $\alpha 1/2$  isoform expression. If  $\alpha$  isoforms  
186 directly contribute to behavioral phenotypes in mice, then increasing their expression may drive  
187 phenotypes in the opposite direction. To test this idea, we created a new mouse line designed  
188 to upregulate SynGAP- $\alpha$  expression *in vivo*. This line, called *Syngap1<sup>+/β\*</sup>*, contained a point  
189 mutation that prevented use of the e19a spliced reading frame (**Fig. 3A-B**), the mechanism  
190 leading to expression of the SynGAP- $\beta$  C-terminal variant (**Fig. 1C**). This design was expected  
191 to force all mRNAs to use the e19b reading frame, leading to an increase in  $\alpha$  variants (and loss  
192 of  $\beta$  expression). This line appeared healthy, bred normally, and resulting offspring were of  
193 expected Mendelian ratios (*Figure 3 - supplement 1C*). The CRISPR-engineered point mutation  
194 had the predicted impact on SynGAP isoform expression. While there was no change in t-  
195 SynGAP expression, there was a copy-number-dependent decrease in  $\beta$  expression, and a  
196 modest, but significant, increase in  $\alpha 2$  expression in neonatal mice and  $\alpha 1$  in young adult mice  
197 (**Fig. 3C; Fig. 1H; Figure 3 -supplement 1A**). These animals were then evaluated in behavioral  
198 paradigms sensitive to *Syngap1* haploinsufficiency. Homozygous *Syngap1<sup>β\*/β\*</sup>* mice exhibited  
199 significantly less horizontal activity in the open field (**Fig. 3D**), and also took longer to express  
200 behavioral evidence of seizure (**Fig. 3E**). Further, they expressed no change in freezing levels

201 during remote contextual memory recall (**Fig. 3F**). Unexpectedly, homozygous  $\beta^*$  mice exhibited  
202 improved learning in the Morris water maze (**Fig. 3G**), with normal memory expression during  
203 the probe test (*Figure 3 -supplement 1B*). Thus, a significant increase in  $\alpha$  isoform expression  
204 (*in the presence of nearly absent  $\beta$ ; Fig. 1H*) protected against seizure and improved behavioral  
205 measures associated with cognitive function, such as learning during spatial navigation.  
206

207 Given the observation of seizure protection and improved learning in *Syngap1* $^{\beta^*/\beta^*}$  mice, we  
208 were curious if the impact of the  $\beta$  allele was penetrant in a *Syngap1* heterozygous (*Syngap1* $^{+/-}$ )  
209 background. This is important given that *Syngap1* heterozygous mice, which model genetic  
210 impacts of SYNGAP1 haploinsufficiency in humans, have seizures and significant cognitive  
211 impairments. To test this idea, we crossed *Syngap1* $^{+/\beta^*}$  and *Syngap1* $^{+/-}$  lines, which yielded  
212 offspring with four distinct genotypes: *Syngap1* $^{++}$ , *Syngap1* $^{+/\beta^*}$ , *Syngap1* $^{+/-}$ , *Syngap1* $^{-/\beta^*}$  (**Fig.**  
213 **4A**). We first measured SynGAP protein in each of the four genotypes. In general terms,  
214 offspring from this cross expressed changes in SynGAP protein levels that were predicted by  
215 the known impact of each allele. For example, the effect of the *Syngap1* null allele (by  
216 comparing *Syngap1* $^{++}$  to *Syngap1* $^{+/-}$  samples) was to cause a significant reduction in t-SynGAP,  
217 and each of the measured C-terminal isoforms compared to *Syngap1* $^{++}$  (WT) animals (**Fig. 4B-C**,  
218 *Figure 4 - supplement*). The effect of the *Syngap1*  $\beta^*$  allele was to increase both  $\alpha 1$  and  $\alpha 2$   
219 expression, and decrease  $\beta$  expression, whether the *Syngap1* null allele was present or absent,  
220 and these effects were also present at two developmental time points (**Fig. 4B-C**, *Figure 4 -*  
221 *supplement*). Given these results, we next performed behavioral analyses on all four  
222 genotypes. Results on behavioral endophenotypes were consistent with changes in SynGAP  
223 protein. For example, the *Syngap1* null allele impaired performance in each of the three  
224 behavioral tests performed. Comparing *Syngap1* $^{+/-}$  to *Syngap1* $^{-/\beta^*}$  animals revealed an increase  
225 in horizontal distance in the open field, faster time to seizure, and reduced freezing during  
226 remote contextual fear recall (**Fig. 4D-F**; two-way ANOVA; null (-) allele,  $p<0.05$ ). These results  
227 replicate many past studies demonstrating the sensitivity of these behaviors to *Syngap1*  
228 haploinsufficiency in mice [12, 18, 20, 21, 27, 32, 33]. Interestingly, for both open field and  
229 seizure threshold tests, the presence of  $\beta^*$  allele significantly improved measures in both WT  
230 (*Syngap1* $^{++}$ ) and *Syngap1* heterozygous (*Syngap1* $^{+/-}$ ) backgrounds (**Fig. 4D-E**; two-way  
231 ANOVA;  $\beta^*$  allele,  $p<0.01$ ; interaction of null and  $\beta$  alleles,  $p>0.5$ ). These findings were  
232 consistent with behavioral results from homozygous  $\beta^*$  mice in the prior study (**Fig. 3F-G**) and  
233 demonstrated that these two behavioral tests are sensitive to the presence of a single  $\beta^*$  allele.  
234 Also consistent with the prior study in *Syngap1* $^{\beta^*/\beta^*}$  mice, the  $\beta^*$  allele had no impact on freezing  
235 during remote contextual fear recall in either WT or *Syngap1* heterozygous backgrounds (**Fig.**  
236 **4F**). Thus, the  $\beta^*$  allele partially rescued phenotypes caused by *Syngap1* heterozygosity.  
237

238 *Alpha 1 C-Terminal Isoform Function is Required for Cognitive Function and Seizure Protection*  
239 The results obtained from *Syngap1* IRES-TD and  $\beta^*$  mouse lines indicated that a respective  
240 decrease, or increase, in  $\alpha 1/2$  isoform expression impaired, or improved, behavioral phenotypes  
241 known to be sensitive to *Syngap1* heterozygosity. However, it is also possible that  
242 compensatory changes in  $\beta$  expression underlies these phenotypes. This alternative is unlikely,  
243 given that  $\alpha$  and  $\beta$  expression is anticorrelated in both mouse lines. Thus, for  $\beta$  to drive  
244 phenotypes, its expression would need to be both anti-cognitive and pro-seizure, which is  
245 inconsistent with isoform expression patterns in *Syngap1* $^{+/-}$  mice (*Figure 2 -supplement 1A*),  
246 where all protein variants are reduced by half. To directly test the hypothesis that behavioral  
247 phenotypes are sensitive to the presence of  $\alpha$  isoforms, we attempted to create a third mouse  
248 line with point mutations that selectively impacted  $\alpha$  isoforms, with minimal effect to SynGAP- $\beta$ .  
249 We took advantage of a known molecular function exclusive to SynGAP- $\alpha 1$ . This C-terminal

250 variant is the only isoform that expresses a PDZ-binding motif (PBM). Importantly, cell-based  
251 studies have shown that the  $\alpha 1$ -exclusive PBM imparts unique cellular functions to this isoform  
252 [17, 34], such as the ability to become enriched at the post-synaptic density through liquid-liquid  
253 phase separation (LLPS). Past studies have shown that mutating the PBM disrupts the ability of  
254 SynGAP to regulate synapse structural and functional properties [25, 26], including  
255 glutamatergic synapse transmission and dendritic spine size. Before this mouse could be  
256 engineered, we had to first identify PBM-disrupting point mutations within the  $\alpha 1$  coding  
257 sequence that were silent within the open reading frames of the remaining C-terminal isoforms.  
258 *In silico* predictions and prior studies [25, 34] suggested that a double point mutation within the  
259  $\alpha 1$  PBM could meet these requirements (**Fig. 5A-B**). To test this prediction, we introduced these  
260 point mutations into a cDNA that encoded the PBM and then tested how this impacted PDZ  
261 binding. Using an established cell-based assay that reports PDZ binding between the SynGAP  
262 PBM and PSD95 [34], we found that these point mutations had a large effect on SynGAP-PDZ  
263 binding. When expressed individually in HeLa cells, PSD95-tRFP localized to the cytoplasm,  
264 while a SynGAP fragment containing the coiled-coil domain and  $\alpha 1$  C-tail (EGFP-CC $\alpha 1$ ) was  
265 enriched in the nucleus (**Fig. 5C-E**). The co-expression of these two proteins led to SynGAP  
266 localization into the cytoplasm. However, this shift in localization did not occur when PBM point  
267 mutations were present (**Fig. 5D-E**), indicating that the selected amino acid substitutions  
268 severely impaired binding to the PDZ domains. Moreover, co-immunoprecipitation in  
269 heterologous cells indicated that the point mutations in the PBM disrupted the direct association  
270 of full-length SynGAP- $\alpha 1$  with PSD95 (*Figure 5 -supplement 1A-B*). Finally, these point  
271 mutations also reduced synaptic enrichment of exogenously expressed SynGAP- $\alpha 1$  fragments  
272 in cultured forebrain neurons (*Figure 5 -supplement 1C-E*).  
273

274 Based on this evidence, we introduced the PBM-disrupting point mutations into the final exon of  
275 the mouse *Syngap1* gene through homologous recombination (**Fig. 5A, F-H**). Both  
276 heterozygous and homozygous PBM mutant animals (hereafter *Syngap1*<sup>+/PBM</sup> or  
277 *Syngap1*<sup>PBM/PBM</sup>) were viable, appeared healthy, and had no obvious dysmorphic features. We  
278 observed Mendelian ratios after interbreeding *Syngap1*<sup>+/PBM</sup> animals (*Figure 5 -supplement 1F*),  
279 demonstrating that disrupting the PBM had no impact on survival. Western blot analysis of  
280 forebrain homogenates isolated from *Syngap1*<sup>+/PBM</sup> or *Syngap1*<sup>PBM/PBM</sup> mutant animals  
281 demonstrated no difference in t-SynGAP protein levels using antibodies that detect all SynGAP  
282 splice variants (**Fig. 5I-J**). Moreover, using isoform-selective antibodies [35], we observed  
283 normal expression of SynGAP- $\beta$  and SynGAP- $\alpha 2$  isoforms (**Fig. 5I-J**). A reduced signal of  
284 ~60% was observed in samples probed with  $\alpha 1$ -specific antibodies. However, we also observed  
285 a similarly reduced signal in heterologous cells expressing a cDNA encoding the mutant PBM  
286 (*Figure 5 -supplement 1G-I*), indicating that these antibodies have reduced affinity for the  
287 mutated  $\alpha 1$  motif. Together, these data strongly suggest that the  $\alpha 1$  variant is expressed  
288 normally in *Syngap1*<sup>PBM/PBM</sup> animals. This interpretation was supported by RNA-seq data, where  
289 normal levels of mRNA containing the  $\alpha 1$  reading frame were observed in brain samples (*Figure*  
290 *5 -supplement 1J*). These data, combined with the observation of no change in total SynGAP  
291 protein expression in *Syngap1*<sup>PBM/PBM</sup> samples (**Fig. 5I-J**), strongly support the conclusion that  
292 the PBM-disrupting point mutations do not change the expression levels of the major SynGAP  
293 C-terminal splice variants, including those containing the PBM. Thus, this animal model is  
294 suitable for understanding the putative biological functions mediated by  $\alpha 1$ -specific splicing.  
295

296 Given the disruption to SynGAP- $\alpha 1$  PBM, we sought to understand how disrupting this  
297 functional motif impacted previously defined features of SynGAP at excitatory postsynapses.  $\alpha 1$   
298 is believed to be anchored within the PSD in part through PBM binding to PDZ domain  
299 containing proteins. However, SynGAP molecules multimerize in vivo and it is currently

300 unknown if this results in homo- or hetero-multimerization. Thus, it is unclear how a functional  
301 disruption to one isoform generally impacts native SynGAP complexes at synapses. t-SynGAP  
302 levels were reduced in PSD fractions prepared from the hippocampus of *Syngap1*<sup>PBM/PBM</sup> mice  
303 (**Fig. 6A**). Importantly, a corresponding increase in t-SynGAP was observed in the triton soluble  
304 synaptosomal fraction in these mice, further supporting the observation of reduced t-SynGAP  
305 levels in the PSD. We observed similar reductions in t-SynGAP levels within the PSD and  
306 ERK1/2 signaling was elevated in neurons cultured from *Syngap1*<sup>PBM/PBM</sup> mice (**Fig. 6B**). Acute  
307 treatment with the NMDAR antagonist APV normalized SynGAP levels in both PSD  
308 preparations and normalized ERK1/2 phosphorylation (**Fig. 6B**). Similar treatments also  
309 normalized enrichment of SynGAP in dendritic spines and surface expression of GluA1 in  
310 neurons derived from *Syngap1*<sup>PBM/PBM</sup> mice (**Fig. 6 C, D**). These results indicate that  
311 endogenous PBM binding regulates an NMDAR-dependent process within excitatory synapses.  
312

313 Blocking NMDAR activity in *Syngap1*<sup>PBM/PBM</sup> neurons prevented alterations in SynGAP levels at  
314 postsynapses (**Fig. 6A-D**). This suggested that the PBM regulates SynGAP-specific functions in  
315 the PSD. However, SynGAP- $\alpha$ 1 undergoes LLPS and this mechanism is thought to facilitate the  
316 organization of the PSD [34]. Thus, disrupted SynGAP post-synaptic levels could also be  
317 attributable to altered structural organization of the PSD. To determine if the PBM contributes to  
318 the organization of macromolecular complexes within excitatory synapses, we  
319 immunoprecipitated PSD95 from neurons obtained from either WT or *Syngap1*<sup>PBM/PBM</sup> mutant  
320 neurons. These neurons were treated with APV to avoid the confounds of elevated NMDAR  
321 signaling. These samples were then analyzed by mass spectrometry to determine how  
322 disrupting SynGAP-PDZ binding impacted the composition of PSD95 macromolecular  
323 complexes. In general, we found only minor differences in the abundance of proteins that  
324 comprise PSD95 complexes when comparing samples from each genotype (**Fig. 7A**). Only 1  
325 out of ~161 proteins (from 133 distinct genes) known to be present within PSD95 complexes  
326 [36] met our threshold for significance, although there were modest changes in proteins with  
327 structurally homologous PBMs (Type-1 PDZ ligands), such as Iqseq2 and Dlgap3 (**Fig. 7B**).  
328 However, the vast majority of related PBM-containing proteins were not different in mutant  
329 neurons, including NMDAR subunits and TARPs (**Fig. 7C**). Consistent with the mass  
330 spectrometry analysis, immunoblot analyses found no changes in TARPs or LRRTM2 in  
331 isolated PSDs from *Syngap1*<sup>PBM/PBM</sup> mice (**Fig. 7D-G**). Although PDZ binding was disrupted,  
332 SynGAP protein levels were also unchanged within PSD95 complexes, a result consistent with  
333 PSD and synapse localization measurements in APV-treated neurons derived from  
334 *Syngap1*<sup>PBM/PBM</sup> mice (**Fig. 6B-C**). These results indicate that SynGAP interacts with PSD95 in a  
335 non-PDZ-dependent manner. In support of this interpretation, there is significant overlap  
336 between the interactomes of PSD95 [36] and SynGAP [37] macromolecular complexes (**Fig.**  
337 **7H**). Thus, within intact postsynapses, SynGAP and PSD95 interact, as part of a  
338 macromolecular complex, through binding to common protein intermediaries. Together, these  
339 data suggest that SynGAP PBM binding to PDZ domains is not a major factor promoting the  
340 organization of PSD95 macromolecular complexes or the PSD. Rather, the PBM appears to  
341 regulate SynGAP-specific mechanisms that control signaling through NMDARs.  
342

343 Given that altering the SynGAP PBM disrupts signaling through NMDARs, we hypothesized that  
344 hippocampal CA1 LTP would be disrupted in *Syngap1*<sup>PBM/PBM</sup> mice. The within-train facilitation of  
345 responses across the seven theta bursts used to induce LTP did not differ between genotypes  
346 (**Fig. 8A**), indicating that standard measures of induction, including NMDAR channel activation,  
347 were not impacted by PBM mutations. However, short-term plasticity (STP; **Fig. 8C, D**) and LTP  
348 (**Fig. 8B, E**) were both reduced in *Syngap1*<sup>PBM/PBM</sup> mice. The ratio of LTP/STP was no different  
349 between genotypes (**Fig. 8F**). Blocking NMDAR channel function is known to disrupt both STP  
350 and LTP [38]. However, a key measure of NMDA channel function was normal in PBM mutant

351 mice (**Fig. 8A**). Thus, these data are consistent with the idea that disrupting SynGAP-PDZ  
352 binding impairs signaling normally induced downstream of synaptic NMDAR activation. Synaptic  
353 plasticity, such as LTP, is thought to contribute importantly to multiple forms of learning and  
354 memory. As such, we next measured performance of WT and *Syngap1*<sup>PBM/PBM</sup> mice in a variety  
355 of learning and memory paradigms that have previously shown sensitivity in *Syngap1* mouse  
356 models, including IRES-TD and  $\beta^*$  lines. Behavioral analysis in this line revealed a significant  
357 increase in horizontal locomotion in the open field test (**Fig. 8G**), a significantly reduced seizure  
358 threshold (**Fig. 8H**), and significantly reduced freezing during retrieval of a remote contextual  
359 fear memory (**Fig. 8I**). Moreover, we also observed impaired acquisition during Morris water  
360 maze learning (**Fig. 8J**). Together, these behavioral data indicate that the PBM within SynGAP-  
361  $\alpha$ 1 splice forms is critical for learning and memory, as well as protecting against seizure.  
362

363 *Alpha1/2 C-Terminal Isoform expression or function predicts changes in excitatory synapse*  
364 *function*

365 Behavioral results from IRES-TD and PBM mice were consistent with each other, and also  
366 consistent with a reduction in all SynGAP isoforms occurring in *Syngap1* conventional  
367 heterozygous KO mice. These three mouse lines share a common molecular feature – reduced  
368 expression or function of SynGAP- $\alpha$ 1 isoforms (**Fig. 1F-I**). Prior studies have shown that  
369 exogenously expressed SynGAP- $\alpha$ 1 is a negative regulator excitatory synapse function [25, 39].  
370 Thus, we hypothesized that IRES-TD and PBM mouse lines would express elevated excitatory  
371 synapse function, while *Syngap1* <sup>$\beta^*/\beta^*$</sup>  mice, which have enhanced  $\alpha$ 1 expression, would express  
372 reduced synapse function. To test this idea, we performed whole-cell voltage clamp recordings  
373 in acute somatosensory cortex slices derived from all three of these lines because these  
374 neurons have been shown to be sensitive to *Syngap1* heterozygosity in *ex vivo* slice  
375 preparations [21]. PBM mice exhibited a modest increase in *mEPSCs* amplitude and a more  
376 substantial increase in *mEPSC* frequency, two measures consistent with enhanced postsynaptic  
377 function (**Fig. 9A-C**). We also observed increased excitatory synapse function (both *mEPSC*  
378 amplitude and frequency distributions) in IRES-TD mice (**Fig. 9D-F**). The effects on synapse  
379 function from L2/3 SSC neurons observed in these two lines are similar to what has been  
380 reported previously in *Syngap1* <sup>$^{+/-}$</sup>  mice [21]. In contrast, *Syngap1* <sup>$\beta^*/\beta^*$</sup>  mice, which have  
381 significantly elevated  $\alpha$ 1 expression, expressed reduced *mEPSC* amplitude and frequency  
382 measurements relative to littermate control slices (**Fig. 9G-I**), a phenotype consistent with  
383 SynGAP- $\alpha$ 1 overexpression in excitatory neurons [25, 39].  
384

385 **Discussion**

386 In this study, we created three distinct mouse lines, each regulating the expression or function  
387 of SynGAP protein isoforms (**Fig. 1F-I**), without appreciable change in total SynGAP expression  
388 levels. The overall conclusion from this study is that  $\alpha$ -containing SynGAP isoforms promote  
389 cognitive functions that support learning/memory, while also protecting against seizure. It is  
390 important to understand the relationship between SynGAP isoform function and systems-level  
391 manifestations of the different isoforms, such as behavioral expression related to cognitive  
392 function and seizure. It has been shown previously that *Syngap1* C-terminal splicing imparts  
393 distinct cellular functions of SynGAP proteins [22, 24-26]. Thus, targeting endogenous isoform  
394 expression in animal models presents an opportunity to determine to what extent distinct cellular  
395 functions of SynGAP could contribute to various intermediate phenotypes present in *Syngap1*  
396 mouse models. Given that *SYNGAP1* is a well-established NDD gene and LOF mutations are  
397 highly penetrant in the human population [1-3, 5, 6, 8, 40, 41], studying these relationships have  
398 the potential to provide much needed insight into the neurobiology underlying human cognitive  
399 and behavioral disorders that first manifest during development. Second, there is increasing  
400 interest in targeted treatments for patients with *SYNGAP1* disorders due to the penetrance of

401 LOF variants, the relatively homogenous manifestations of the disorder (e.g., cognitive  
402 impairment and epilepsy), and the growing number of patients identified with this disorder [42].  
403 Restoring SynGAP protein expression in brain cells is the most logical targeted treatment for  
404 this disorder because most known patients have *de novo* variants that cause genetic  
405 haploinsufficiency [9]. The most logical therapeutic approach would be to reactivate native  
406 expression of the endogenous gene. However, the findings from this study indicate that targeted  
407 therapies for *SYNGAP1* disorders that enhance expression of  $\alpha$  isoforms may be sufficient to  
408 provide a benefit to patients. Indeed, only a modest upregulation of  $\alpha$ 1/2 expression within a  
409 *Syngap1* heterozygous background was sufficient to improve behavioral deficits commonly  
410 observed in that mouse line (Fig. 4). Third, the discovery that SynGAP- $\alpha$ 1/2 expression/function  
411 is pro-cognitive and provides protection from seizure suggests that these isoforms, and the  
412 cellular mechanisms that they regulate, could be harnessed to intervene in idiopathic cognitive  
413 and excitability disorders, such as neurodegenerative disorders and/or epilepsies with unknown  
414 etiology.  
415

416 Several lines of evidence from this study support the conclusion that SynGAP- $\alpha$  isoform  
417 expression or function promotes cognition and seizure protection. IRES-TD and PBM mouse  
418 lines each had similar learning/memory and seizure threshold phenotypes, with both mouse  
419 lines exhibiting impaired phenotypes related to these two types of behavioral analyses. Indeed,  
420 these two mouse lines also shared a common molecular perturbation - reduced expression or  
421 function of alpha isoform(s). For example, IRES-TD homozygous mice lacked expression of  
422 both  $\alpha$ 1 and  $\alpha$ 2 isoforms and these animals exhibited severe phenotypes, including reduced  
423 post-weaning survival and dramatically elevated horizontal activity in the open field. Additional  
424 phenotypes were also present in heterozygous IRES-TD mice, which underwent more  
425 comprehensive testing because of better survival in the post-weaning period. These additional  
426 phenotypes included reduced seizure threshold and impaired freezing during a remote  
427 contextual fear expression test. PBM homozygous mice had normal expression of SynGAP  
428 protein, but lacked a functional domain present exclusively in  $\alpha$ 1 isoforms, a type-1 PDZ binding  
429 domain. PBM homozygous mice shared phenotypes with IRES-TD mice, including impaired  
430 remote contextual fear expression, elevated horizontal activity in the open field, and a reduced  
431 seizure threshold. These mice also expressed impaired learning during Morris water maze  
432 acquisition. Importantly, these behavioral phenotypes are well established in *Syngap1*  
433 heterozygous mice [16, 18, 20, 32, 33], indicating that SynGAP protein loss-of-function  
434 underlies these abnormalities. Thus, it reasonable to speculate that  $\alpha$  isoform LOF is one  
435 potential mechanism underlying these behavioral abnormalities. Dysregulation of excitatory  
436 synapse function in cortical circuits is one of many possible cellular mechanisms underlying  
437 common phenotypes in IRES-TD and PBM mutant mice lines. Whole cell electrophysiology  
438 experiments from developing cortical neurons *in situ* from each line revealed evidence of  
439 elevated excitatory synapse strength during the known *Syngap1* mouse critical period. Indeed,  
440 elevated excitatory synapse strength in developing forebrain glutamatergic neurons is a major  
441 cellular outcome present in *Syngap1* heterozygous knockout mice [16, 18, 19, 21]. Moreover,  
442 elevated excitatory synapse strength is consistent with impaired cognitive function and reduced  
443 seizure threshold.  
444

445 Studies in the *Syngap1*  $\beta^*$  line also support this interpretation. These mice were devoid of  
446 SynGAP- $\beta$  protein expression, yet we did not observe cellular or behavioral phenotypes  
447 consistent with *Syngap1* heterozygosity. Rather surprisingly, mice lacking SynGAP- $\beta$   
448 expression had intermediate phenotypes that opposed what was commonly observed in  
449 *Syngap1* heterozygous KO mice (and shared by IRES-TD/PBM lines). For example,  $\beta^*$  mice  
450 exhibited improved spatial learning in the Morris water maze, reduced horizontal activity in the

451 open field, and an elevated seizure threshold (evidence of seizure protection). These  
452 phenotypes were modest in effect size, but highly significant. These phenotypes were  
453 reproducible because open field and seizure phenotypes were also present in a separate series  
454 of experiments performed in the *Syngap1* heterozygous background. This demonstrates that the  
455 impact of the  $\beta^*$  allele is penetrant even when expression of isoforms is reduced by half  
456 compared to WT mice. As a result, the  $\beta^*$  allele partially rescued open field and seizure  
457 phenotypes present in *Syngap1<sup>+/−</sup>* mice. For impaired  $\beta$  expression to drive phenotypes,  
458 expression of this isoform would be anticorrelated with cognitive function and seizure protection.  
459 Put another way, reduced  $\beta$  expression would need to enhance phenotypes and increased  
460 expression of these isoforms would need to disrupt them. This outcome is unlikely given that it  
461 is inconsistent with phenotypes observed in *Syngap1<sup>+/−</sup>* mice, which have reduced expression of  
462 all isoforms, including SynGAP- $\beta$ .  
463

464 Phenotypes in  $\beta^*$  mice are likely driven by significantly elevated SynGAP- $\alpha$  expression rather  
465 than reduced SynGAP- $\beta$ . Electrophysiological studies in these mice revealed reduced excitatory  
466 neuron synaptic strength, a finding consistent with exogenously elevated SynGAP- $\alpha 1$   
467 expression [25, 39]. Moreover, these synapse-level results are consistent with seizure  
468 protection observed in  $\beta^*$  mice. Phenotypes in PBM mice also support this hypothesis. This  
469 model does not have altered t-SynGAP expression, or a change in  $\beta$  expression. Yet, the  
470 behavioral- and synapse-level phenotypes are consistent with those observed in IRES-TD and  
471 *Syngap1<sup>+/−</sup>* mice. The observation that  $\alpha$  isoforms promote cognitive function and seizure  
472 protection are consistent with known molecular functions of these isoforms, at least with respect  
473 to regulation of synapse strength and resultant impacts on neural circuit function. For example,  
474  $\alpha 1$  imparts SynGAP with the ability to undergo liquid-liquid phase transitions [34]. This  
475 biophysical process is associated with regulation of Ras signaling in dendritic spines required  
476 for AMPA receptor trafficking that supports use-dependent synapse plasticity [17, 22]. Input-  
477 specific plasticity is crucial during development to sculpt the assembly of neural circuits [43],  
478 while also being important in mature circuits to promote experience-dependent changes in  
479 already-established circuitry [44].  
480

481 A consensus is emerging that baseline synaptic phenotypes related to *Syngap1* gene  
482 expression are dominated by the ability of both  $\alpha 1$  and  $\alpha 2$  isoforms to suppress excitatory  
483 synapse function. Studies from several research groups have shown that SynGAP- $\alpha 1$  is a  
484 negative regulator of excitatory synapse structure and function [17, 22, 25, 26, 39]. In contrast,  
485 the role of  $\alpha 2$  isoform protein function on excitatory synapse structure/function is less clear. One  
486 study suggested that  $\alpha 2$  has an opposing function relative to  $\alpha 1$  within excitatory synapses, with  
487 the former acting as an enhancer, rather than a suppresser, of excitatory synapse function [24].  
488 However, a more recent study demonstrated that  $\alpha 2$  has a similar, albeit less robust ability to  
489 suppress AMPA receptor content within dendritic spines [22], indicating that it too can act as a  
490 negative regulator of synapse function. Our results here support the view that both  $\alpha 1$  and  $\alpha 2$   
491 can act as suppressors of excitatory synapse function. In our studies,  $\alpha 1$  and  $\alpha 2$  were both co-  
492 regulated in the IRES-TD and  $\beta^*$  lines, with both isoforms downregulated in the former and  
493 upregulated in the latter. In both mouse lines, baseline excitatory synapse strength was  
494 inversely proportional to expression levels of  $\alpha 1/2$  isoforms. If  $\alpha 1$  and  $\alpha 2$  had opposing functions  
495 at the synapse level, then co-regulation of both isoforms would be expected to lead to no  
496 significant differences in synapse function.  
497

498 It is important to note that our interpretation that  $\beta^*$  mouse phenotypes are most likely driven by  
499 changes in  $\alpha$  isoforms does not preclude a fundamental role of  $\beta$  in sculpting neural systems, or

500 that reduced expression of this isoform in *Syngap1*<sup>+/−</sup> mice has no role in disease pathobiology.  
501 Rather, our results highlight the importance of endogenous  $\alpha$  isoforms in regulating excitatory  
502 synapse function and associated behavioral outcomes. What is known about the function of  
503 other C-terminal protein variants, such as  $\beta$  and  $\gamma$ ? A recent study suggested that  $\beta$  and  $\gamma$   
504 isoforms lack the ability to regulate excitatory synapse function, further strengthening the idea  
505 that  $\alpha$  isoforms account for *Syngap1*-dependent regulation of excitatory synapse function [22].  
506 However, *Syngap1* is known to regulate additional cellular process beyond regulation of  
507 excitatory synapse function, such as dendritic morphogenesis and patterning *in vivo* [18, 20, 21].  
508 Evidence suggests that all isoforms can regulate dendritic morphogenesis *in vitro*, though  
509 SynGAP- $\beta$  was shown to be a stronger regulator of this process relative to the other C-terminal  
510 isoforms [22]. *In vivo*,  $\beta$  was found to be expressed earlier in development and to be less  
511 enriched in the postsynaptic density compared to other variants [23]. Thus,  $\beta$  is well positioned  
512 to regulate non-synapse related neuronal processes. Future studies will be required to elucidate  
513 the specific cellular functions of non-alpha isoforms and how they contribute to the development  
514 of neural function and behavior. Given the complexities of *Syngap1* regulation on dendritic  
515 morphogenesis [20, 21], and the direct linkage between dendritic morphogenesis and circuit  
516 function in cortex in *Syngap1* mutant animals [21], future studies on the function of individual  
517 isoforms would ideally be carried out *in vivo* in developing animals.

518  
519  
520  
521  
522  
523  
524  
525

526 **Acknowledgements**

527 This work was supported in part by NIH grants from the National Institute of Mental Health  
528 (MH096847 and MH108408 to G.R., MH115005 and MH113949 to M.P.C, and MH105400 to  
529 C.A.M.), the National Institute for Neurological Disorders and Stroke (NS064079 to G.R.), the  
530 Eunice Kennedy Shriver National Institute of Child Health and Human Development (HD089491  
531 to G.L.), the National Institute for Drug Abuse (DA034116 and DA036376 to C.A.M.), the  
532 Spanish Ministerio de Ciencia, Innovación y Universidades (BFU2012-34398, BFU2015-69717-  
533 P, RTI2018-097037-B-100, RYC-2011-08391p and IEDI-2017-00822) and the Catalan  
534 Government (AGAUR SGR14-297 and 2017SGR1776). M.K. was supported by Autism Speaks  
535 Weatherstone Pre-Doctoral fellowship (10646). G.G. was supported by a predoctoral fellowship  
536 from the Spanish Ministerio de Educación (BES-2013-063720). V.A. was supported by a  
537 training Fellowship from Leon and Friends.

538

539 **Author Contributions**

540 M.K. performed experiments, designed experiments, analyzed data, co-wrote the manuscript,  
541 and edited the manuscript. V.A performed experiments, designed experiments, analyzed data,  
542 and edited the manuscript. T.K.C. performed experiments, designed experiments, analyzed  
543 data, and edited the manuscript. C.R. performed experiments, designed experiments and  
544 analyzed data. A.A.L performed experiments, designed experiments, and analyzed data. J.L  
545 designed experiments and analyzed data. B.W. performed experiments, designed experiments,  
546 and analyzed data. N.H. performed experiments and designed experiments. N.G. performed  
547 experiments and designed experiments. A.R. analyzed data. G.G. performed experiments.  
548 Y.A. performed experiments. A.B. designed experiments, analyzed data, and interpreted data.  
549 M.P.K. designed experiments, analyzed data, and interpreted data. G.L. designed experiments,  
550 analyzed data, and interpreted data. C.A.M. designed experiments, interpreted data, and edited  
551 the manuscript. G.R. conceived the study, designed experiments, interpreted data, co-wrote the  
552 manuscript, and edited the manuscript.

553

554 **Declaration of Interests**

555 The authors declare no competing financial interests.

556

557

558

559

560 **Materials & Methods**

561

562 **Animals**

563 This study was performed in strict accordance with the recommendations in the Guide for the  
564 Care and Use of Laboratory Animals of the National Institutes of Health. All of the animals were  
565 handled according to approved institutional animal care and use committee (IACUC) protocols  
566 of The Scripps Research Institute.

567

568 *Syngap1*<sup>PBM</sup> and *Syngap1*<sup>Td</sup> mice were constructed in collaboration with genOway (France). The  
569 targeting vector was electroporated into ES cells derived from the inner cell mass of 3.5 days  
570 old C57BL/6N embryos. Cells were then subjected to negative and/or positive selection(s)  
571 before the presence of the correct recombination event was validated by PCR and Southern  
572 blot. ES cell clones with verified mutations were injected into blastocysts which were implanted  
573 into pseudo-pregnant females to obtain chimeras. Chimeric mice were bred with C57BL/6 Cre-  
574 deleter mice to excise the Neomycin selection cassette and to generate heterozygous mice  
575 carrying the Neo-excised knock-in allele. Progeny were genotyped by PCR. The recombinase-  
576 mediated excision event was further validated by Southern blot using 5' external probes. Knock-  
577 in lines were maintained on C57BL/6J background and bred for 3 generations prior to  
578 experimental use. *Syngap1*<sup>PBM</sup> animals were genotyped using the following primers, which  
579 amplified the locus spanning the LoxP site: Fwd: 5'-ctggttcaaaggctcctggta-3' Rev: 5'-  
580 ctgtttgttctcacctccaggaa-3'. This combination yielded a 61bp product in WT and 120bp product  
581 in knock-in alleles. *Syngap1*<sup>Td</sup> line were genotyped using the primers amplifying the locus  
582 including the TdTomato cassette: Fwd: 5'-AGATCCACCAGGCCCTGAA-3' Rev: 5'-  
583 GTCTTGAACCTCCACCAGGTAGTG-3'

584

585 *Syngap1*- $\beta^*$  mice were constructed in collaboration with the Scripps Research Genetics core  
586 facility. To selectively disrupt SynGAP- $\beta$  expression, exon19a splice acceptor site "AAG" was  
587 mutated into "ACG". To introduce the point mutation, purified CRISPR/Cas9 protein combined  
588 with gRNA and donor DNA was injected to ~100 zygotes and implanted into surrogate mice. A  
589 200 bp PAGE purified ss-oligo repair template centering the CRISPR cut site was used as  
590 donor DNA. Recombination events were detected by PCR and Sanger sequencing of the DNA  
591 isolated from tails of F0 potential founders. This process identified 2 chimeric mice with  
592 evidence of the targeted nucleotide variants. Chimeras were then bred with C57BL6/J and  
593 resultant heterozygous F1 mice were used to start the colony. Because CRISPR carries a risk  
594 of off-target genomic effects, prior to any downstream experiments, this line was further crossed  
595 into C57BL6/J for >3 generations.

596

597 **Transcriptomics**

598 PND7 mice forebrains (Cortex + hippocampus) were immediately removed and stored in  
599 RNAlater (Thermo, AM7020). mRNA was isolated with RNeasy mini kit (74104, Qiagen). RNA  
600 integrity was measured using Agilent 2100 Bioanalyzer (RIN value  $\geq$  9.2 for each sample).  
601 Library preparation and sequencing on the Illumina NextSeq 500 were performed by the Scripps  
602 Florida Genomics Core. De-multiplexed and quality filtered raw reads (fastq) were trimmed  
603 (adaptor sequences) using Flexbar 2.4 and aligned to the reference genome using TopHat  
604 version 2.0.9 (Trapnell et al., 2009). HT seqcount version 0.6.1 was used to generate gene  
605 counts and differential gene expression analysis was performed using Deseq2 (Anders and  
606 Huber, 2010). Deseq2 identified differentially expressed genes (DEGs) with a cutoff of 1.5 fold  
607 change and an adjusted p-value of less than 0.05 (Love et al., 2014). Paired end reads mapped

608 to the first 30 bases of Exon21 was used to determine the ratio of Exon21a (results in SynGAP-  
609  $\alpha 2$ ) vs Exon21b (results in SynGAP- $\alpha 1$ ) splicing events.  
610

## 611 **Cell Culture**

612 Cell lines: HeLa Cells (Kind gift of Michael Farzan) and HEK293T Cells (Kind gift of Joseph  
613 Kissil) were cultured in DMEM media containing 10% fetal bovine serum and  
614 penicillin/streptomycin.  
615

616 Primary forebrain cultures: Dissociated forebrain cultures were prepared from newborn WT and  
617 homozygous littermates of the PBM line as previously described (Bedouin 2012). Briefly,  
618 forebrains were isolated and incubated with a digestion solution containing papain for 25 min at  
619 37 °C. Tissues were washed and triturated in Neurobasal medium containing 5% FBS. Cells  
620 were plated on poly-D-lysine at a density of 1,000 cells per mm<sup>2</sup>. Cultures were maintained in  
621 Neurobasal A media (Invitrogen) supplemented with B-27 (Invitrogen) and Glutamax  
622 (Invitrogen). At DIV4 cells were treated with FuDR to prevent glial expansion. The cells were  
623 sparsely labeled by administration of AAVs (CamKII.Cre, 10<sup>4</sup>vg/ml, Addgene # 105558-AAV9  
624 and CAG.Flex.EGFP, 10<sup>8</sup>vg/ml, Addgene #28304-PHPeB) at DIV 9-10 and processed for  
625 experiments 10-11 days later.  
626

## 627 ***In situ* Colocalization Assay**

628 HeLa cells were plated on glass coverslips and transfected with PSD95-tRFP (Plasmid #52671,  
629 Addgene) and/or EGFP-tagged SynGAP C-terminal constructs (EGFP-CC $\alpha 1$  or EGFP-CCPBM  
630 plasmids (made in house) were co-transfected into HeLa cells using lipofectamine 2000  
631 according to manufacturer instructions. Cells were then fixed with 4% PFA and washed multiple  
632 times with PBS prior to mounting with Prolong Gold with DAPI (P36931, Thermo). Confocal  
633 stacks spanning entire cells were obtained using UPlanSApo 100 $\times$  1.4 NA oil-immersion  
634 objective mounted on Olympus FV1000 laser-scanning confocal microscope using Nyquist  
635 criteria for digital imaging. Maximum intensity projections were used for the analysis. Nuclei of  
636 cells were defined by DAPI staining, and the EGFP-CC nuclear localization was calculated as  
637 the EGFP (colocalized with nucleus) / EGFP (within entire cell perimeter).  
638

## 639 **PSD95-SynGAP Co-IP Assay**

640 PSD95-tRFP (Plasmid #52671, Addgene) and/or full length EGFP-SynGAP $\alpha 1$ /PBM (made in  
641 house) plasmids were transfected in HEK293T cells using Lipofectamine 2000. Cells were  
642 homogenized with Pierce IP Lysis buffer (87787, Thermo) containing protease & phosphatase  
643 inhibitors. Lysates were then incubated for 2hrs at RT with 1.5mg Dynabeads (10004D,  
644 Thermo) functionalized with 10ug of anti-PSD95 (Thermo, MA1-045) or IgG control (ab18415,  
645 Abcam). After extensive washing, immunoprecipitated proteins were eluted with Leammeli  
646 buffer at 70C for 10min with agitation. Eluted proteins were detected via western blot using  
647 PSD-95 (Thermo, MA1-045) and SynGAP (D20C7, CST) antibodies. 10% of the input and 20%  
648 of IP elute were used for each sample.  
649

## 650 ***In Vitro* Treatments**

651 To silence neuronal activity and block NMDAR signaling, cultures were treated for 3hrs with 1  
652  $\mu$ M TTX and 200  $\mu$ M APV. To induce chemical LTP, Cells were thoroughly washed and perfused  
653 with basal ECS (143 mM NaCl, 5 mM KCl, 10 mM HEPES (pH 7.42), 10 mM Glucose, 2 mM  
654 CaCl<sub>2</sub>, 1 mM MgCl<sub>2</sub>, 0.5  $\mu$ M TTX, 1  $\mu$ M Strychnine, and 20  $\mu$ M Bicuculline) for 10 min. Then  
655 magnesium free ECS containing 200  $\mu$ M Glycine (or 10  $\mu$ M Glycine for weak cLTP) was applied  
656 for 10 min. Cells were then washed with and incubated in basal ECS for additional 10 min prior  
657 to downstream application.  
658

659 **Subcellular Fractionation**

660 From tissue: Frozen hippocampi or cortex were homogenized using a Teflon-glass homogenizer  
661 in ice-cold isotonic solution (320 mM sucrose, 50 mM Tris pH 7.4, phosphatase & protease  
662 inhibitors). The homogenate was then centrifuged at 1,000g for 10min at 4 °C. The supernatant  
663 (S1) was centrifuged at 21,000g for 30min. The pellet (P2) was resuspended in isotonic buffer  
664 and layered on top of a discontinuous sucrose density gradient (0.8M, 1.0M or 1.2M sucrose in  
665 50mM Tris pH 7.4, +inhibitors) and centrifuged at 82,500g for 2hr at 4°C. The interface of 1.0M  
666 and 1.2M sucrose was collected as a synaptosomal fraction. Synaptosomes were diluted using  
667 50mM Tris pH7.4 (+inhibitors) to bring the sucrose concentration to 320mM. The diluted  
668 synaptosomes were then pelleted by centrifugation at 21000g for 30min at 4°C. The  
669 synaptosome pellet was then resuspended in 50mM Tris pH 7.4 and then mixed with an equal  
670 part 2% Triton-X (+inhibitors). This mixture was incubated at 4 °C with rotation for 10min  
671 followed by centrifugation at 21,000xg for 20min to obtain a supernatant (Syn/Tx) and a pellet  
672 (PSD).

673

674 From primary culture: Cultured neurons (DIV 18-21), were homogenized by passage through  
675 22G needle 10 times in ice-cold isotonic buffer (320 mM sucrose, 50 mM Tris, protease &  
676 phosphatase inhibitor mix). Homogenates were centrifuged at 1,000 × g for 10 min at 4 °C. The  
677 supernatant (S1) was centrifuged at 15,000 × g for 20 min at 4 °C to obtain the crude  
678 membrane (P2 fraction). The P2 pellet was resuspended with ice-cold hypotonic buffer (50 mM  
679 Tris, protease & phosphatase inhibitor mix) and was incubated for 30 min at 4C. Then the  
680 sample was centrifuged 21,000 x g for 30min to obtain synaptic plasma membrane (SPM)  
681 fraction. SPM is reconstituted in hypotonic buffer then equal volume of hypotonic buffer with 2%  
682 Triton-X was added and the mixture was incubated 15min on ice. Lysates were centrifuged at  
683 21,000g for 30 min at 4 °C to obtain a soluble fraction (Syn/Tx) and a pellet (PSD), which was  
684 resuspended in 50 mM Tris containing 0.5% SDS. To completely solubilize PSD fraction, we've  
685 briefly sonicated and heated samples to 95 °C for 5min.

686

687 **Immunoblotting**

688 Protein lysates were extracted from the hippocampi or cortices of adult mice and dissected in  
689 ice-cold PBS containing Phosphatase Inhibitor Cocktails 2 and 3 (Sigma-Aldrich, St. Louis, MO)  
690 and Mini-Complete Protease Inhibitor Cocktail (Roche Diagnostics) and immediately  
691 homogenized in RIPA buffer (Cell Signaling Technology, Danvers, MA), and stored at -80 °C.  
692 Sample protein concentrations were measured (Pierce BCA Protein Assay Kit, Thermo  
693 Scientific, Rockford, IL), and volumes were adjusted to normalize microgram per microliter  
694 protein content. For phospho-protein analysis, *in vitro* cultures were directly lysed with laemmeli  
695 sample buffer, sonicated and centrifuged to minimize DNA contamination. 10 µg of protein per  
696 sample were loaded and separated by SDS-PAGE on 4-15 % gradient stain-free tris-glycine  
697 gels (Mini Protean TGX, BioRad, Hercules, CA), transferred to low fluorescence PVDF  
698 membranes (45 µm) with the Trans-Blot Turbo System (BioRad). Membranes were blocked with  
699 5% powdered milk (BSA for phospho-proteins) in TBST and probed overnight at 4 °C with the  
700 following primary antibodies: Pan-SynGAP (Thermo, PA1-046), SynGAP-α1 (Millipore, 06-900),  
701 SynGAP-α2 (abcam, ab77235), SynGAP-β (Kind gift of Rick Huganir), PSD-95 (Thermo, MA1-  
702 045), Synaptophysin (Novus, NB300-653), pERK (CST, 9106), ERK (CST, 4696), GluA1  
703 (Millipore, MAB2263), phospho-serine845 GluA1 (Millipore, AB5847), TARP (Millipore,  
704 Ab9876), LRRTM2 (Thermo Pierce, PA521097).

705

706 **Immunocytochemistry**

707 For SynGAP – PSD95 colocalization, neurons were fixed in 4% PFA, 4% sucrose for 5 min at  
708 RT and treated with MetOH for 15min at -20°C. The cells were then washed with PBS and  
709 permeabilized in PBS 0.2% TritonX-100 for 10 min. Samples were then blocked for 1 hr and

710 probed for SynGAP (D20C7, CST) and PSD95 (MA1-045, Abcam) overnight. After PBS  
711 washes, samples were probed with appropriate secondary antibodies for 1 hr in the dark at  
712 room temperature. The coverslips were then washed, mounted (Prolong Glass) and cured.  
713 Confocal stacks were obtained. For analysis, maximum intensity Z projection was obtained from  
714 each confocal image. Individual synapses were traced as PSD95 positive puncta selected using  
715 an arbitrary threshold which was kept constant across all images. Mean SynGAP and PSD95  
716 signals were measured from individual synapses. *For surface GluA1 staining*, neurons were  
717 immediately fixed in ice-cold pH 7.2 4% PFA, 4% sucrose for 20 min on ice. Then, samples  
718 were washed three times with ice-cold PBS and blocked for 1 hr min in PBS containing 10%  
719 NGS. Cells were then incubated overnight with a primary antibody targeting the extracellular N  
720 terminus of GluA1 (MAB2263, Millipore) and then washed with 10% goat serum twice to remove  
721 excess primary antibody. After PBS washes, Alexa dye-conjugated secondary antibodies were  
722 added for 1 hr in the dark at room temperature. The coverslips were then washed, mounted  
723 (Prolong Glass) and cured. Surface GluA1 levels were measured from manually traced  
724 individual dendritic spines from maximum intensity Z projection images using EGFP channel  
725 (cell fill). All confocal stacks were obtained for 6–12 individual fields from multiple coverslips per  
726 culture with UPlanSApo 100 $\times$  1.4 NA oil-immersion objective mounted on Olympus FV1000  
727 laser-scanning confocal microscope using Nyquist criteria for digital imaging. 40-80  $\mu$ m  
728 stretches of secondary dendrites in neurons with pyramidal morphology were imaged.

#### 729 **PSD95 Immunoprecipitation and Mass Spectrometry**

730 Harvested neurons were lysed in DOC lysis buffer (50 mM Tris (pH 9), 30 mM NaF, 5 mM  
731 sodium orthovanadate, 20 mM  $\beta$ -glycerol phosphate, 20  $\mu$ M ZnCl<sub>2</sub>, Roche complete, and 1%  
732 sodium deoxycholate). The lysate was then centrifuged at 35,000 RPM for 30 minutes at 4°C  
733 and lysate containing 1 mg of protein was incubated with 2  $\mu$ g Psd95 antibody (Neuromab,  
734 catalog # 75-048) at 4°C overnight with rotation. The following day, IPs were incubated with  
735 Dynabeads protein G (Thermo Fisher Scientific, catalog # 10004D) for 2 hours at 4 degrees  
736 Celsius. IPs were then washed three times with IP wash buffer (25 mM Tris (pH 7.4), 150 mM  
737 NaCl, 1 mM EDTA, and 1% Triton X-100). Dynabeads were re-suspended in 2X LDS sample  
738 buffer and incubated at 95 degrees Celsius for 15 minutes for elution. The eluate was  
739 incubated with DTT at a final concentration of 1 mM at 56°C for 1 hour followed by a 45-minute  
740 room temperature incubation with Iodoacetamide at a final concentration of 20 mM.

741 Samples were loaded onto 4 – 12% Bis-Tris gels and separated at 135V for 1.5 hours. Gels  
742 were stained with InstantBlue (Expedeon, catalog # 1SB1L) to visualize bands. The heavy and  
743 light chains of Immunoglobulin were manually removed. Gels were then destained using 25%  
744 ethanol overnight. Gel lanes were cut, individual gel slices were placed into 96 well plates for  
745 destaining, and peptide digestion was completed at 37 degrees Celsius overnight. Peptides  
746 were extracted with acetonitrile, dried down, and then desalted using stage tips. All LC-MS  
747 experiments were performed on a nanoscale UHPLC system (EASY-nLC1200, Thermo  
748 Scientific) connected to an Q Exactive Plus hybrid quadrupole-Orbitrap mass spectrometer  
749 equipped with a nanoelectrospray source (Thermo Scientific). Samples were resuspended in  
750 10uL of Buffer A (0.1% FA) and 2uL were injected. Peptides were separated by a reversed-  
751 phase analytical column (PepMap RSLC C18, 2  $\mu$ m, 100  $\text{\AA}$ , 75  $\mu$ m X 25 cm) (Thermo  
752 Scientific). Flow rate was set to 300 nL/min at a gradient starting with 3% buffer B (0.1% FA,  
753 80% acetonitrile) to 38% B in 110 minutes, then ramped to 75% B in 1 minute, then ramped to  
754 85% B over 10 minutes and held at 85% B for 9 minutes. Peptides separated by the column  
755 were ionized at 2.0 kV in the positive ion mode. MS1 survey scans for DDA were acquired at  
756 resolution of 70k from 350 to 1,800 m/z, with maximum injection time of 100 ms and AGC target  
757 of 1e6. MS/MS fragmentation of the 10 most abundant ions were analyzed at a resolution of  
758 17.5k, AGC target 5e4, maximum injection time 65 ms, and an NCE of 26. Dynamic exclusion  
759

760 was set to 30 s and ions with charge 1 and >6 were excluded. The maximum pressure was set  
761 to 1,180 bar and column temperature was constant at 50°C. Proteome Discoverer 2.2 (Thermo  
762 Fisher Scientific) was used to process MS data and analyzed using Sequest HT against Uniprot  
763 mouse databases combined with its decoy database. With respect to analysis settings, the  
764 mass tolerance was set 10 parts per million for precursor ions and 0.02 daltons for fragment  
765 ions, no more than two missed cleavage sites were allowed, static modification was set as  
766 cysteine carbamidomethylation, and oxidation of methionine was set as a dynamic modification.  
767 False discovery rates (FDRs) were automatically calculated by the Percolator node of Proteome  
768 Discoverer with a peptide and protein FDR cutoff of 0.01. Label free quantification was  
769 performed using Minora node in Proteome Discoverer. Abundances of identified PSD95  
770 interacting proteins in WT and mutant neurons were compared using relative abundances such  
771 that proteins with a fold change in abundance ratio of > 2.0 or < 0.5 were considered to be  
772 differentially associated to PSD95.

### 773 **Hippocampal LTP and Extracellular Recordings**

774 Acute transverse hippocampal slices (350  $\mu$ m) were prepared using a Leica Vibroslicer (VT  
775 1000S), as described previously (Babayan et al., 2012). Slices were cut into ice cold, choline  
776 chloride artificial cerebral spinal fluid (ACSF) containing (in mM) 110 choline chloride, 2.5 KCl,  
777 1.25 NaH<sub>2</sub>PO<sub>4</sub>, 5 MgSO<sub>4</sub>, 25 NaHCO<sub>3</sub>, 25 glucose, 11.6 ascorbic acid, and 3.1 pyruvic acid  
778 and rinsed at room temperature for ~3 min in a high magnesium aCSF solution containing: 124  
779 NaCl, 3 KCl, 1.25 KH<sub>2</sub>PO<sub>4</sub>, 5 MgSO<sub>4</sub>, 26 NaHCO<sub>3</sub>, and 10 dextrose. Slices were then  
780 transferred to an interface recording chamber maintained at 31±1°C, oxygenated in 95% O<sub>2</sub>/  
781 5% CO<sub>2</sub> and constantly perfused (60-80 ml/h) with normal ACSF (in mM; 124 NaCl, 3 KCl, 1.25  
782 KH<sub>2</sub>PO<sub>4</sub>, 1.5 MgSO<sub>4</sub>, 2.5 CaCl<sub>2</sub>, 26 NaHCO<sub>3</sub>, and 10 dextrose). Slices equilibrated in the  
783 chamber for approximately 2 hours before experimental use. Field excitatory postsynaptic  
784 potentials (fEPSPs) were recorded from CA1b stratum radiatum using a single glass pipette (2-3  
785 M $\Omega$ ). Bipolar stainless-steel stimulation electrodes (25  $\mu$ m diameter, FHC) were positioned at  
786 two sites (CA1a and CA1c) in the apical Schaffer collateral-commissural projections to provide  
787 activation of separate converging pathways of CA1b pyramidal cells. Pulses were administered  
788 in an alternating fashion to the two electrodes at 0.05 Hz using a current that elicited a 50%  
789 maximal response. After establishing a 10-20 min stable baseline, long-term potentiation (LTP)  
790 was induced in the experimental pathway by delivering 7 'theta' bursts, with each burst  
791 consisting of four pulses at 100 Hz and the bursts themselves separated by 200 msec (i.e.,  
792 theta burst stimulation or TBS). The stimulation intensity was not increased during TBS. The  
793 control pathway received baseline stimulation (0.05Hz) to monitor the health of the slice. The  
794 fEPSP slope was measured at 10–90% fall of the slope and all values pre- and post- TBS  
795 normalized to mean values for the last 10 min of baseline recording. Baseline measures for all  
796 groups included paired-pulse facilitation and input/output curves.

797

### 798 **Ex vivo whole-cell electrophysiology**

799 Acute coronal slices (350  $\mu$ m) were prepared from 10-14 days old mice for 3 mouse lines. Ice-  
800 cold cutting solution was used for slice preparation and contained the following (in mM): 119  
801 NaCl, 2.5 KCl, 1.3 MgSO<sub>4</sub>, 2.5 CaCl<sub>2</sub>, 1 NaH<sub>2</sub>PO<sub>4</sub>, 11 D-glucose and 26.3 NaHCO<sub>3</sub>, pH 7.4,  
802 300-310 mOsm bubbled with 95%CO<sub>2</sub> and 5%O<sub>2</sub>. The slices were then warmed to 37°C for an  
803 hour approximately in standard artificial cerebrospinal fluid (aCSF), composed of (mM): 125  
804 NaCl, 2.5 KCl, 24 NaHCO<sub>3</sub>, 2 CaCl<sub>2</sub>, 1.25 NaH<sub>2</sub>PO<sub>4</sub>, 2 MgSO<sub>4</sub>, and 10 D-Glucose, and  
805 equilibrated with 95 % O<sub>2</sub> and 5 % CO<sub>2</sub> (pH 7.4, ~300 mOsm). Following this, slices were  
806 maintained in bubbled aCSF at room temperature until transferred to a submerged-type  
807 recording chamber (Warner Instruments, Hamden, CT). All experiments were performed at  
808 32°C±2 (perfusion rate of 2-3 mL/min). Whole-cell patch clamp experiments were conducted  
809 from visually identified L2/3 neurons using infrared DIC optics. L2/3 excitatory cells were

810 identified by their soma shape and their location ~ 150  $\mu$ M below the L1-L2 boundary. Regular  
811 spiking was confirmed in current clamp and miniature excitatory postsynaptic current (mEPSC)  
812 were recorded from identified cells for 5 sweeps each lasting a minute, using the following  
813 internal solution (in mM): 120 CsCl, 10 K-HEPES, 10 EGTA, 5 QX314-Br, 4 Mg-ATP, 0.3 Na-  
814 GTP, 4 MgCl<sub>2</sub> (pH 7.3, 290-295 mOsm). Perfusion solution aCSF was supplemented with 100  
815  $\mu$ M picrotoxin and 1  $\mu$ M TTX. Cells with access resistance >20 M $\Omega$  or were unstable (>20 %  
816 change) were discarded from further analysis. Recordings were made using borosilicate glass  
817 pipettes (3-6 M $\Omega$ ; 0.6 mm inner diameter; 1.2 mm outer diameter; Harvard Apparatus). All  
818 signals were amplified using Multiclamp 700B (Molecular Devices, Sunnyvale, CA), filtered at 4  
819 KHz, digitized (10 KHz), and stored on a personal computer for off-line analysis. Analog to  
820 digital conversion was performed using the Digidata 1440A system (Molecular Devices). Data  
821 acquisition and analyses were performed using pClamp 11.2software package (Clampex and  
822 Clampfit programs; Molecular Devices) and minianalysis (Synaptosoft). The events were  
823 considered mini-EPSCs if the peak of an event was >5 pA.

824

## 825 **Behavior**

826 At weaning, four mice were randomly allocated to one cage with respect to genotype with males  
827 and females being housed separately. Randomization of cage allocation was restricted in that,  
828 as much as possible, mice from the same litter were placed in different cages so that no single  
829 litter was overrepresented in any single experiment. Cages utilized for behaviors contained  
830 cardboard pyramidal-shaped huts with two square openings on opposing sides of the hut for the  
831 purposes of environmental enrichment and to assist with transfers from home cages to  
832 behavioral apparatuses. All mice were handled for several minutes on three consecutive days  
833 prior to commencement of behavioral testing. Tails were marked for easy identification and  
834 access from home cages during testing. Experimenters were blind to mouse genotype while  
835 conducting all tests.

836

837 **Flurothyl-induced seizures:** Flurothyl-induced seizure studies were performed based on prior  
838 studies with some modifications [16, 18, 45]. Briefly, experiments were conducted in a chemical  
839 fume hood. Mice were brought to the experimental area at least 1 h before testing. To elicit  
840 seizures, individual mice were placed in a closed 2.4-L Plexiglas chamber and exposed to 99%  
841 Bis (2,2,2-trifluoroethyl) ether (Catalog# 287571, Sigma-Aldrich, St. Louis, MO). The flurothyl  
842 compound was infused onto a filter paper pad, suspended at the top of the Plexiglas chamber  
843 through a 16G hypodermic needle and tube connected to a 1 ml BD glass syringe fixed to an  
844 infusion pump (KD Scientific, Holliston, MA, USA, Model: 780101) at a rate of 0.25 ml/min. The  
845 infusion was terminated after the onset of a hind limb extension that usually resulted in death.  
846 Cervical dislocation was performed subsequently to ensure death of the animal. Seizure  
847 threshold was measured as latency (s) from the beginning of the flurothyl infusion to the  
848 beginning of the first myoclonic jerk.

849

850 **Morris water maze:** Mice were run in a standard comprehensive Morris water maze paradigm  
851 including a cue test with a visual platform and an acquisition protocol with a hidden platform. All  
852 phases of the paradigm were run in a dedicated water maze room in the Scripps Florida Mouse  
853 Behavior Core. A water maze system including a plastic white opaque pool (Cat# ENV-594M-W,  
854 Med Associates), measuring ~122cm diameter at the water surface, supported by a stand  
855 (ENV-593M-C) and equipped with a floor insert (ENV-595M-FL) covering a submerged heater  
856 was utilized for all water maze experimentation. An adjustable textured platform (17.8 cm  
857 diameter, ENV-596M) was placed atop the floor insert in one of two different quadrants,  
858 depending on the specific phase of the paradigm (NW quadrant for initial training and probe test  
859 and SE quadrant for reversal training and probe tests), for mice to escape the water. Water  
860 temperatures were controlled to 22.5 ± 0.5 °C using a built-in heater and monitored with a digital

861 temperature probe. This water temperature motivated the mice to escape the water without  
862 eliciting hypothermic conditions. The tank was emptied, cleaned and refilled once every three  
863 days to avoid unsafe accumulation of bacteria. Water was made opaque by the addition of a  
864 white opaque non-toxic paint (Crayola) forcing mice to utilize extra-maze cues when locating the  
865 hidden platform (0.5 cm beneath the surface of the water). These spatial cues (large black  
866 cardboard circle, star, square, white X on black background) were placed on the walls of the  
867 room at different distances from the pool. The pool edge was demarcated with directional units  
868 (W, N, E, S) to aid assignment of invisible platform “quadrants” to the pool arena outlined by the  
869 video tracking system. Various strip lights were positioned on the walls near the ceiling to allow  
870 for a moderate level of lighting (200 lux), enough for the mice to see the extra-maze cues  
871 adequately without eliciting undue anxiety. Thirty minutes prior to commencement of daily trials,  
872 the lights and heater were turned on, and mouse home cages were placed on heating pads on a  
873 rack in the water maze room to provide a warm place for the mice between trials. Cage nestlets  
874 were replaced with strips of paper towels to better facilitate drying after trials. Mice were  
875 monitored during trials for signs of distress and swimming competence. None of the mice tested  
876 had swimming issues, and floating was discouraged with gentle nudges. Mice received four  
877 trials per day during cue and acquisition phases and one trial per day for probe trials. Three  
878 cages (12 mice) were run at a time such that ITIs for each day lasted about 20 minutes with trial  
879 duration lasting until the mouse found the platform or a maximum of 60 s. Each trial commenced  
880 when the mouse was automatically detected in the pool by the tracking system (Ethovision,  
881 Noldus). Each mouse was lowered into the pool facing its edge at one of the four directional  
882 units (W, N, E, S) in a clockwise manner, with the first of the four trials starting closest to the  
883 platform (“NW quadrant”), which was positioned in the central area of the quadrant dictated by  
884 the tracking system. This same series of daily trial commencements were followed for all mice  
885 for each of the cue tests, acquisition protocol, and reversal protocol. If the mouse did not locate  
886 the platform in 60 s, the experimenter’s hand guided them to the platform. Because the mice are  
887 eager to escape the water, the mice quickly learned to follow hand direction to the platform,  
888 minimizing physical manipulation of the animals during the trials. Mice were allowed 15 seconds  
889 on the platform at the end of each trial before being picked up, dried with absorbent wipes, and  
890 placed back into their warmed home cage.

891  
892 On the first day of testing, mice were given a cue test with the platform positioned just above the  
893 surface of the water and a metal blue flag placed upon it for easy visual location of the platform.  
894 This test allows for detection of individual visual and swimming-related motor deficits and allows  
895 the mice to habituate to the task (climbing on the platform to escape the water). The platform  
896 was placed in a different location for each of the four trials with spatial cues removed by  
897 encirclement of the pool with a white plastic curtain.

898  
899 On the next day, acquisition trials began with the hidden platform remaining in the same location  
900 (“NW quadrant”) for all trials/days and the curtain drawn back for visibility of the spatial cues.  
901 Several measures (distances to platform) and criteria to reach the platform (approximately 90%  
902 success rate, approximately 20 second latency to find platform) during the acquisition phases  
903 were recorded and achieved before mice were deemed to have learned the task. The  
904 performances of the four trials were averaged for each animal per day until criteria were met.  
905

906 Open field test: Naive mice were individually introduced into one of eight adjacent open field  
907 arenas for 30 min and allowed to explore. Open field arenas consisted of custom made clear  
908 acrylic boxes (43 x 43 x 32h cm) with opaque white acrylic siding surrounding each box 45 x 45  
909 x 21.5h cm to prevent distractions from activities in adjacent boxes. Activity was monitored with  
910 two CCTV cameras (Panasonic WV-BP334) feeding into a computer equipped with Ethovision  
911 XT 11.5 for data acquisition and analyses. A white noise generator (2325-0144, San Diego

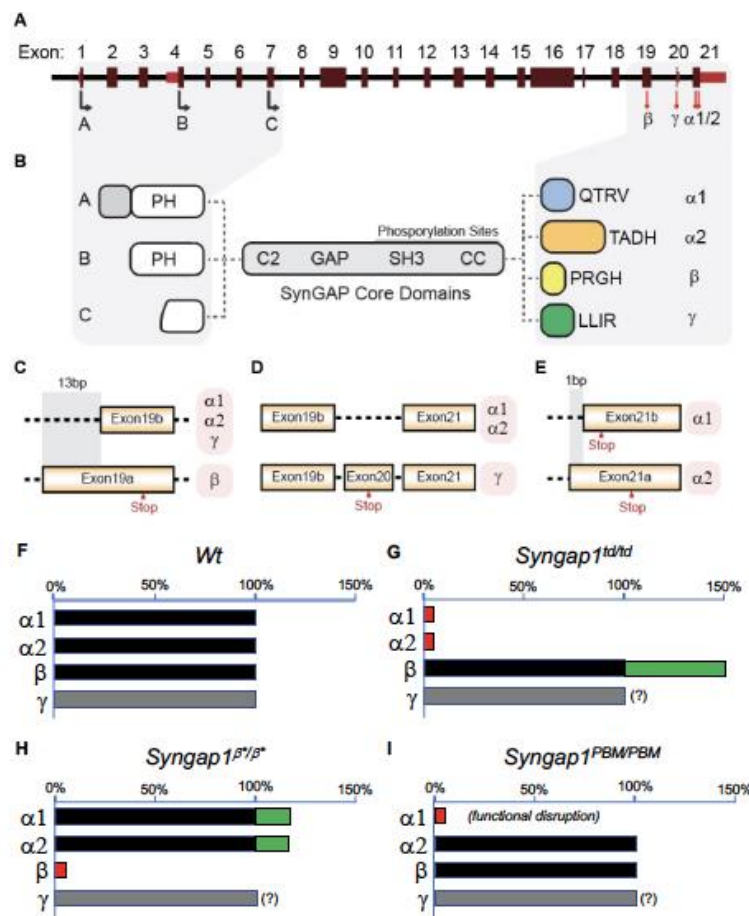
912 Instruments) was set at 65 dB to mask external noises and provide a constant noise level.  
913 Fluorescent linear strip lights placed on each of the four walls of the behavioral room adjacent to  
914 the ceiling provided a lower lighting (200 lux) environment than ceiling lighting to encourage  
915 exploration.

916  
917 *Contextual fear conditioning:* A dedicated fear conditioning room in the TSRI Florida Mouse  
918 Behavior Core contains four fear conditioning devices that can be used in parallel. Each  
919 apparatus was an acrylic chamber measuring approximately 30 x 30 cm (modified Phenotyper  
920 chambers, Noldus, Leesburg, VA). The top of the chamber is covered with a unit that includes a  
921 camera and infrared lighting arrays (Noldus, Ethovision XT 11.5, Leesburg, VA) for monitoring  
922 of the mice. The bottom of the chamber is a grid floor that receives an electric shock from a  
923 shock scrambler that is calibrated to 0.40 mA prior to experiments. The front of the chamber has  
924 a sliding door that allows for easy access to the mouse. The chamber is enclosed in a sound-  
925 attenuating cubicle (Med Associates) equipped with a small fan for ventilation. Black circular,  
926 rectangular and white/black diagonal patterned cues were placed outside each chamber on the  
927 inside walls of the cubicles for contextual enhancement. A strip light attached to the ceilings of  
928 the cubicles provided illumination. A white noise generator (~65 dB) was turned on and faced  
929 toward the corner of the room between the cubicles. The fear conditioning paradigm consisted  
930 of two phases, training, followed by testing 1 and 26, or 30 d thereafter. The 4.5 min training  
931 phase consisted of 2.5 min of uninterrupted exploration. Two shocks (0.40 mA, 2 s) were  
932 delivered, one at 2 min 28 s, the other at 3 min and 28 s from the beginning of the trial. During  
933 testing, mice were placed into their designated chambers and allowed to roam freely for 5 min.  
934 Immobility durations (s) and activity (distances moved (cm)) during training and testing were  
935 obtained automatically from videos generated by Ethovision software. Activity suppression ratio  
936 levels were calculated: 0-2 min activity during testing/0-2 min activity during training + testing.

937  
938

939 **Figure Legends**

940



941  
942

943 **Figure 1 – Schematic of *Syngap1* alternative splicing and summary of isoform expression**  
944 **in three new *Syngap1* mutant mouse lines.** (A) Map showing alternative use of exons in N-  
945 and C-terminal isoforms. N-terminal variants are constituted via use of different start codons in  
946 exon 1, 4 or 7. Exon 4 is present only in B-SynGAP. C-terminal isoforms originate from use of  
947 different splice acceptors in exon 19 and 21. SynGAP-α1 contains a type-1 PDZ ligand (QTRV).  
948 Structure/function relationships of α2, β, γ isoforms remain largely unknown. (B) Schematics of  
949 SynGAP isoforms & protein domains. α and β isoforms include full Pleckstrin Homology (PH)  
950 domain. In C-SynGAP, this domain is truncated. Core regions common to all isoforms include  
951 C2, GAP (GTPase Activating Protein), Src Homology 3 (SH3)-binding, and coiled-coil (CC)  
952 domains. Multiple phosphorylation sites are present downstream of the GAP domain. (C-E)  
953 Schematics describing C-terminal splicing events producing distinct isoforms. (F-I) Summary of  
954 Wt and three new *Syngap1* mutant mouse lines each with distinct targeted alleles that disrupt  
955 the function or expression of SynGAP C-terminal isoforms. Bars represent expression levels of  
956 each C-terminal protein isoform relative to each Wt littermate control. Primary data for  
957 expression levels can be found in subsequent figures.

958  
959

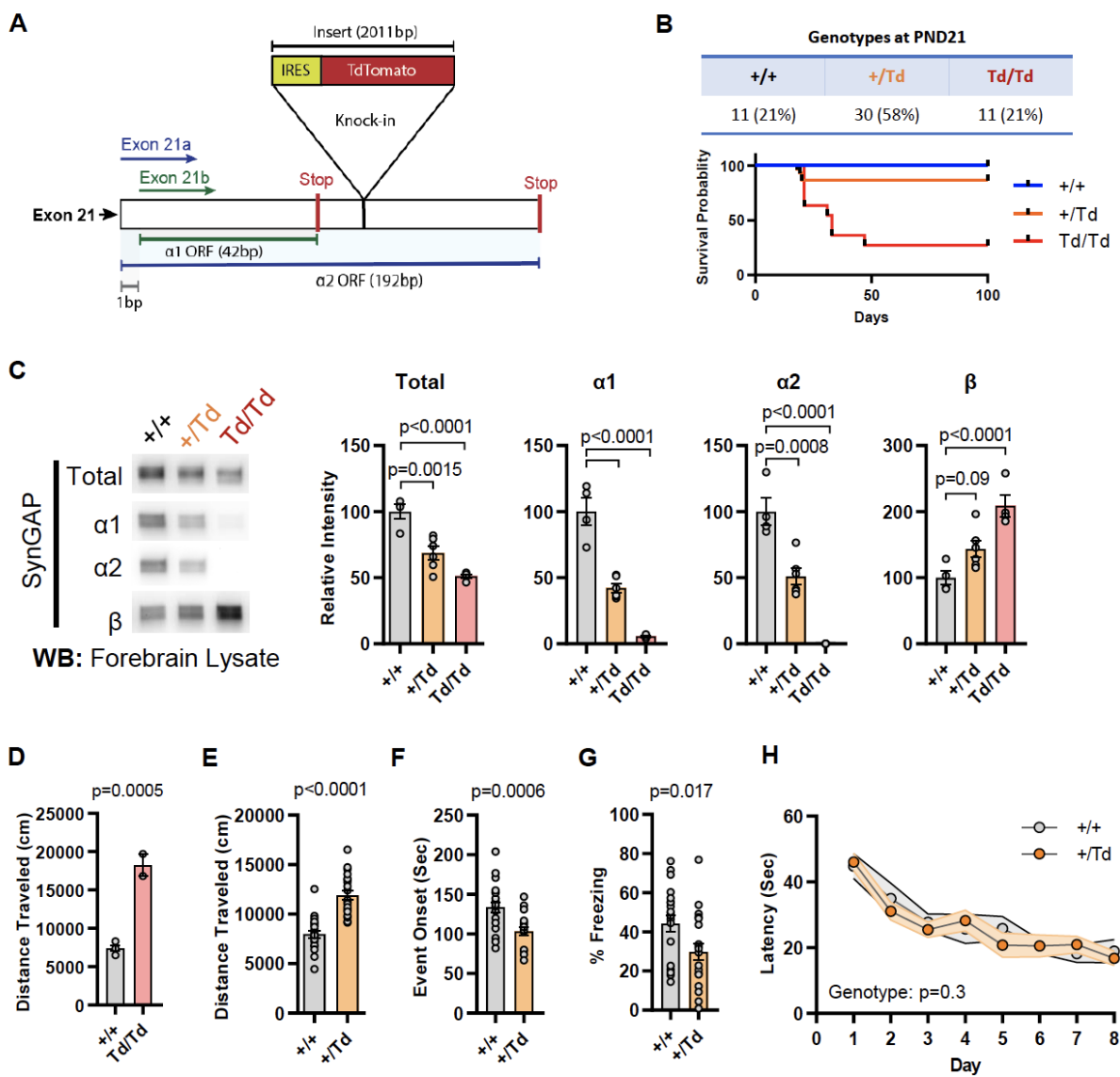
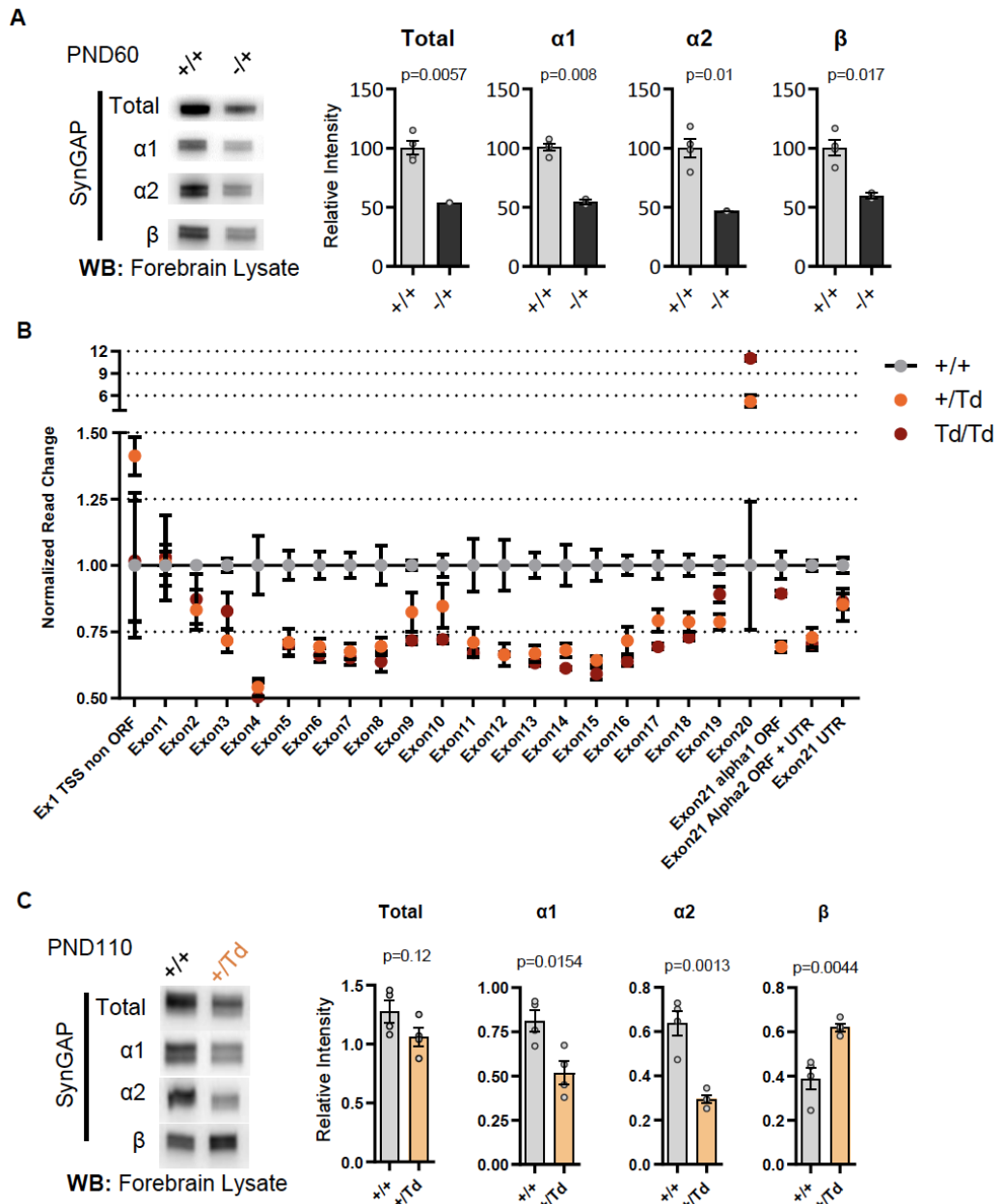


**Figure 2 – Design and characterization of *Syngap1* IRES-TdTomato knock-in mice.**

**(A)** IRES-Tdtomato insertion site in relation to α1 and α2 open reading frames. **(B)** Genotype ratios and survival probability following heterozygous breeding. **(C)** Representative western blots showing expression levels of total SynGAP and individual isoforms. Quantification of forebrain expression levels measured by western blot analysis. Relative intensity of bands normalized to total protein signal. Only α1 signal is significantly changed. ANOVA with Tukey's multiple comparisons test,  $F(2, 14) = 24.86$ ,  $n=5$ ,  $p<0.0001$  **(D)** Quantification of total distance traveled in open field test in adult WT or Td/Td mice. Unpaired t-test  $t(4)=10.42$ . Note that very few homozygous Td/Td mouse survived through adulthood. **(E)** Quantification of total distance traveled in open field test in adult WT or +/Td mice. Unpaired t-test  $t(18)=9.007$  **(F)** Latency of event onset was measured as the time taken to 1st clonus (seizure onset). Unpaired t-test:  $t(18)=2.588$ . **(G)** Percent freezing in remote contextual fear memory paradigm. Unpaired t-test:  $t(41)=2.49$  **(H)** Plots demonstrating latency to find platform across days in Morris Water Maze training. Linear mixed model for repeated measures.  $n=9-12$ , +/+ vs +/Td,  $p=0.3$

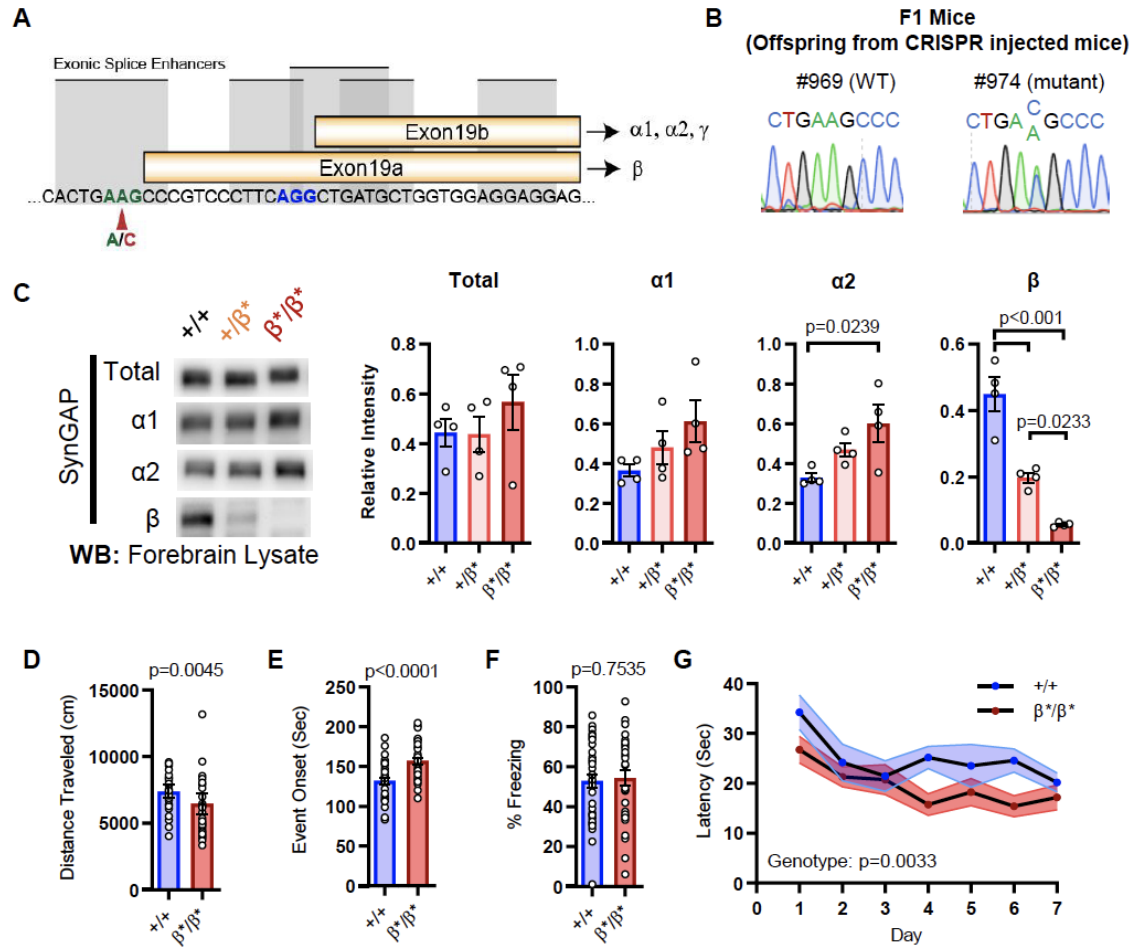
960  
961  
962  
963  
964  
965  
966  
967  
968  
969  
970  
971  
972  
973  
974  
975  
976



977  
978  
979  
980  
981  
982  
983  
984  
985  
986  
987

## Figure 2 - Supplement

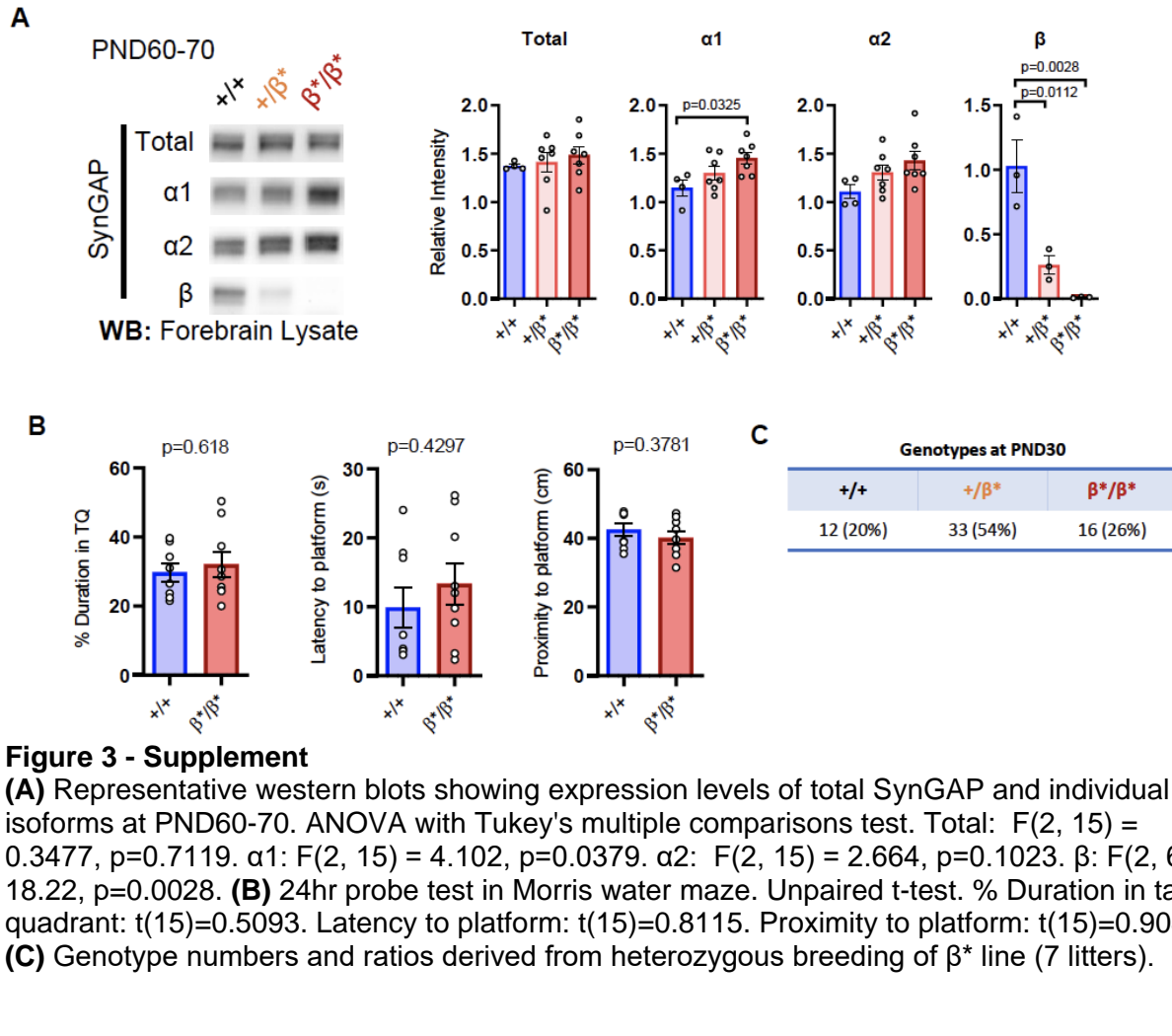
**(A)** Representative western blots demonstrating total SynGAP and isoform expression level in forebrain lysates from *Syngap1*<sup>+/+</sup> and *Syngap1*<sup>+/-</sup> mice. Relative intensity of bands normalized to total protein signal. Statistical significance is determined by unpaired t-test. Total:  $t(4)=5.403$ ,  $\alpha 1$ :  $t(4)=9.044$ ,  $\alpha 2$ :  $t(4)=4.473$ ,  $\beta$ :  $t(4)=3.931$  **(B)** *Syngap1* exon usage in +/+, +/Td, and Td/Td mice. **(C)** Representative western blots showing expression levels of total SynGAP and individual isoforms at PND110 from in +/+ and +/Td mice. Unpaired t-test. Total:  $t(6)=1.784$ ,  $\alpha 1$ :  $t(6)=3.351$ ,  $\alpha 2$ :  $t(6)=5.678$ ,  $\beta$ :  $t(6)=4.425$

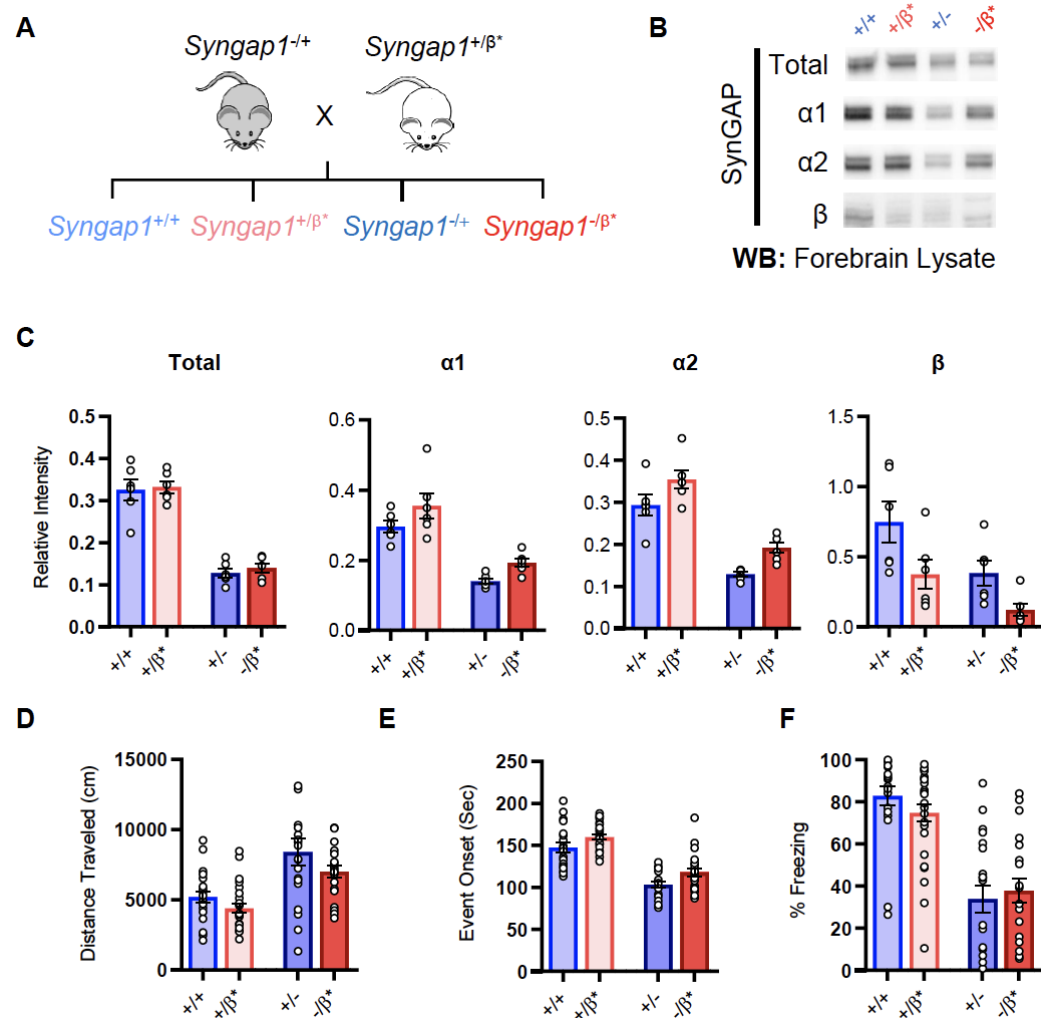


988  
989  
990  
991  
992  
993  
994  
995  
996  
997  
998  
999  
1000  
1001  
1002  
1003  
1004  
1005  
1006  
1007  
1008

### Figure 3 - Design and characterization of *Syngap1<sup>β\*</sup>* knock-in mice.

**(A)** Alternative use of exon19 in distinct splicing events. Exon19 can be spliced into 2 frames shifted by 13 bp. Use of early splice acceptor (green) results in a frameshift and expresses β isoform. Use of the late splice acceptor (blue) allows expression of all other SynGAP C-terminal variants. To specifically disrupt SynGAP-β, a point mutation (A to C) was introduced to the early splice acceptor (indicated with red arrow). **(B)** Sequence trace of *Syngap1<sup>β\*/+</sup>* mice obtained via crossing F0 founders to wild-type mice. Mutation site exhibits equal levels of A and C signal in sequence trace indicating heterozygosity. **(C)** Representative western blots showing expression levels of total SynGAP and individual isoforms at PND7. Relative intensity of bands normalized to total protein signal. ANOVA with Tukey's multiple comparisons test. Total:  $F(2, 9) = 0.7427$ ,  $p=0.5029$ . α1:  $F(2, 9) = 2.391$ ,  $p=0.147$ . α2:  $F(2, 9) = 5.333$ ,  $p=0.0297$ . β:  $F(2, 9) = 42.53$ ,  $p<0.0001$ . **(D)** Quantification of total distance traveled in OFT.  $+/+$  (n=36),  $β/β$  (n=32); Mann-Whitney U=346,  $p=0.0045$ . **(E)** Seizure threshold was measured as the time taken to reach three separate events of 1st clonus (event onset) during the procedure. Unpaired t-test:  $t(66)=4.237$ . **(F)** Percent freezing in remote contextual fear memory paradigm. % Freezing:  $t(66)=0.3153$ . **(G)** Plots demonstrating latency to find platform across days in Morris Water Maze training session. Statistical significance was determined by using linear mixed model for repeated measures. Genotype:  $F(1, 15)=12.22$ ,  $p=0.0033$





1019  
1020 **Figure 4 –Characterization of offspring derived from *Syngap1<sup>+/-</sup>* and *Syngap1<sup>β<sup>+/</sup></sup>* cross-  
1021 breeding. (A) Breeding scheme for offspring genotypes for *Syngap1<sup>+/-</sup>* and *Syngap1<sup>+/β<sup>+</sup></sup>* lines.  
1022 (B) Representative western blots showing expression levels of total SynGAP and individual  
1023 isoforms at PND7 for all genotypes. (C) Quantification of B. Two-way ANOVA with Tukey's  
1024 multiple comparison test. **Total:** (-) allele F(1, 20)=146.3, p<0.0001; β\* allele F(1, 20)=0.3344,  
1025 p=0.5696. Allelic Interaction F(1, 20)=0.03191, p=0.8600. **α1:** (-) allele F(1, 20)=56.01,  
1026 p<0.0001; β\* allele F(1, 20)=7.009, p=0.0155; Allelic Interaction F(1, 20)=0.02397, p=0.8785.  
1027 **α2:** (-) allele F(1, 20)=81.79, p<0.0001; β\* allele F(1, 20)=11.92, p=0.0025; Allelic Interaction  
1028 F(1, 20)=0.0044, p=0.9479. **β:** (-) allele F(1, 20)=9.149, p=0.0067; β\* allele F(1, 20)=9.676,  
1029 p=0.0055; Allelic Interaction F(1, 20)=0.3027, p=0.5883. (D) Quantification of total distance  
1030 traveled in open field test. Two-way ANOVA with Tukey's multiple comparison test. (-) allele F(1,  
1031 86)=28.85, p<0.0001; β\* allele F(1, 86)=4.132, p=0.0452; Allelic Interaction F(1, 86)=0.2951,  
1032 p=0.5884 (E) Latency of event onset was measured as the time taken to 1st clonus (seizure  
1033 onset). Two-way ANOVA with Tukey's multiple comparison test. (-) allele F(1, 82)=91.71,  
1034 p<0.0001; β\* allele F(1, 82)=8.967, p=0.0036; Allelic Interaction F(1, 82)=0.07333, p=0.7872 (F)  
1035 Percent freezing in remote contextual fear memory paradigm. Two-way ANOVA with Tukey's  
1036 multiple comparison test. (-) allele F(1, 86)=69.37, p<0.0001; β\* allele F(1, 86)=0.1544,  
1037 p=0.6953; Allelic Interaction F(1, 86)=1.392, p=0.2414.  
1038  
1039**

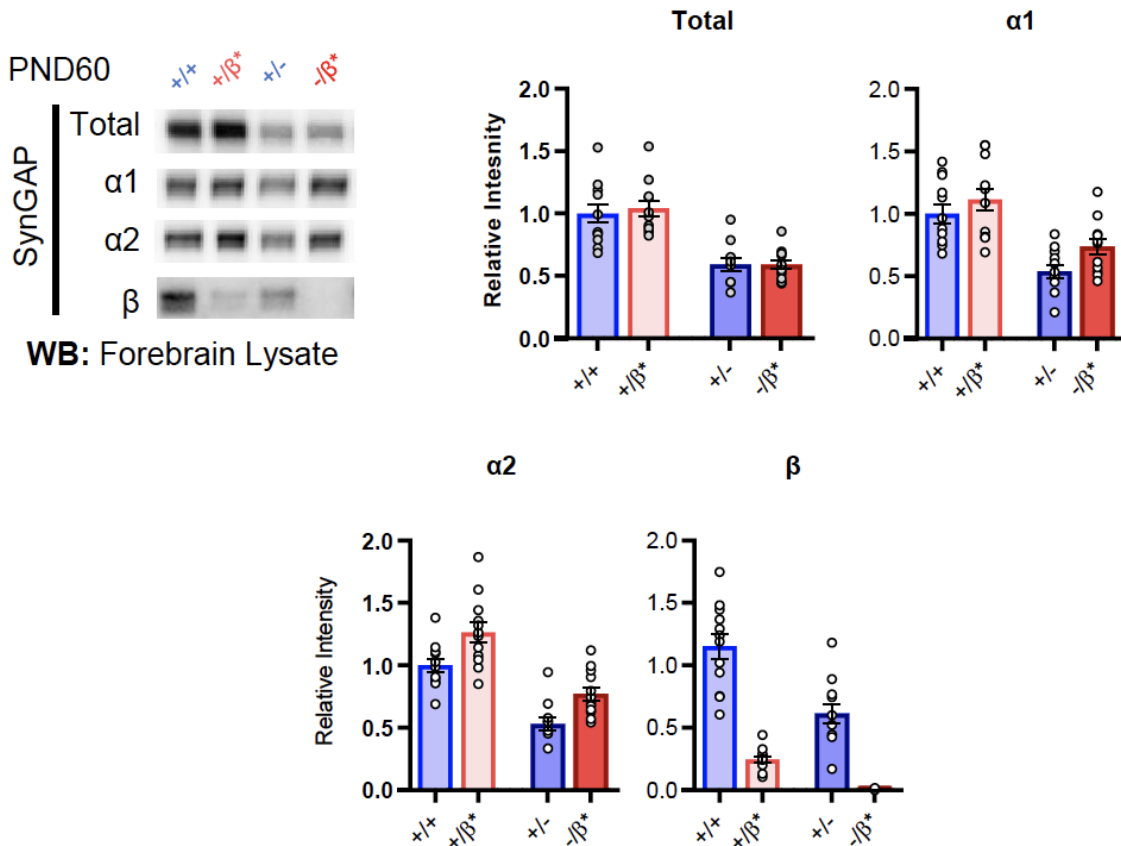
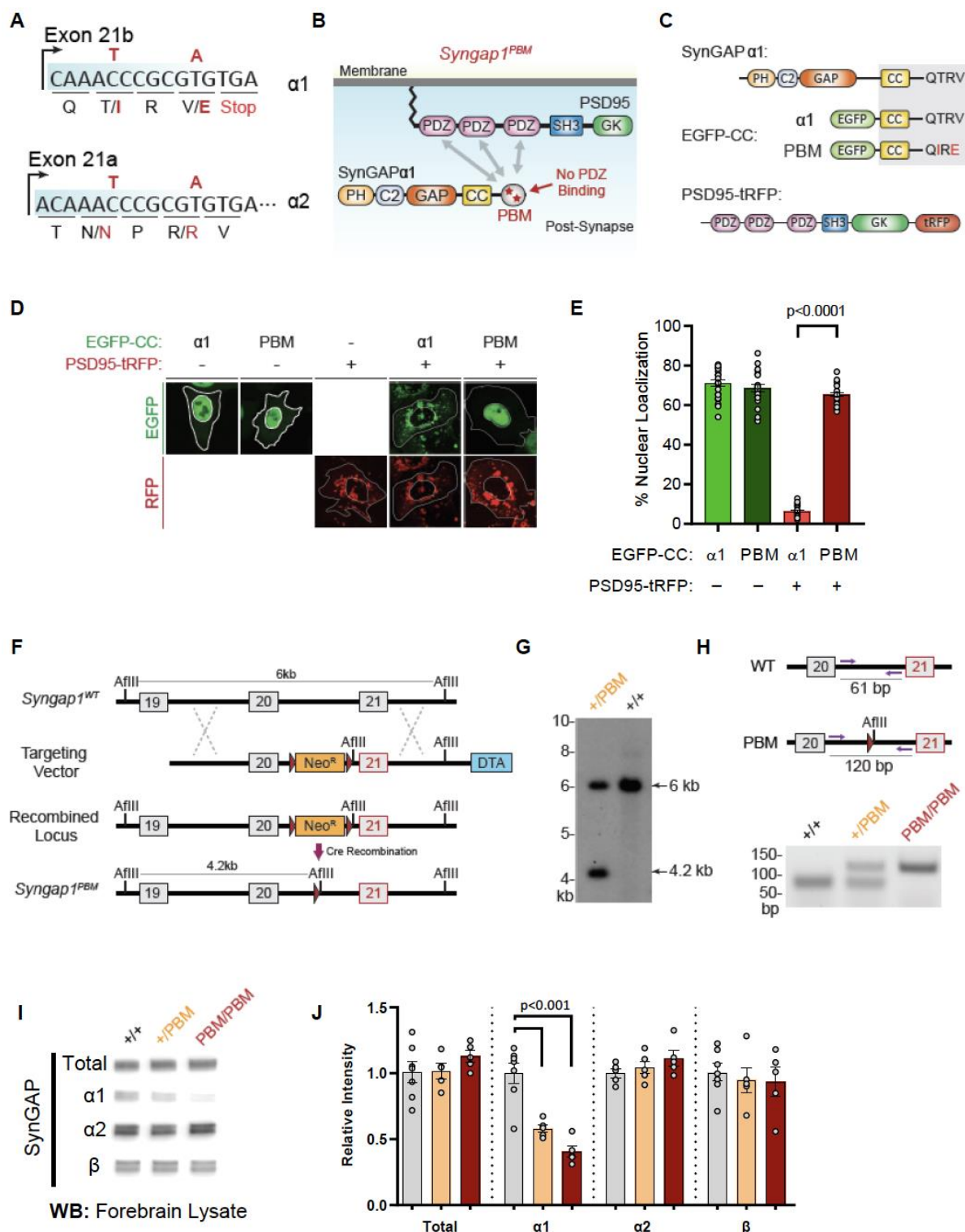


**Figure 4 - Supplement**

Representative western blots showing expression levels of total SynGAP and individual isoforms at PND60 for all genotypes. Two-way ANOVA with Tukey's multiple comparison test.

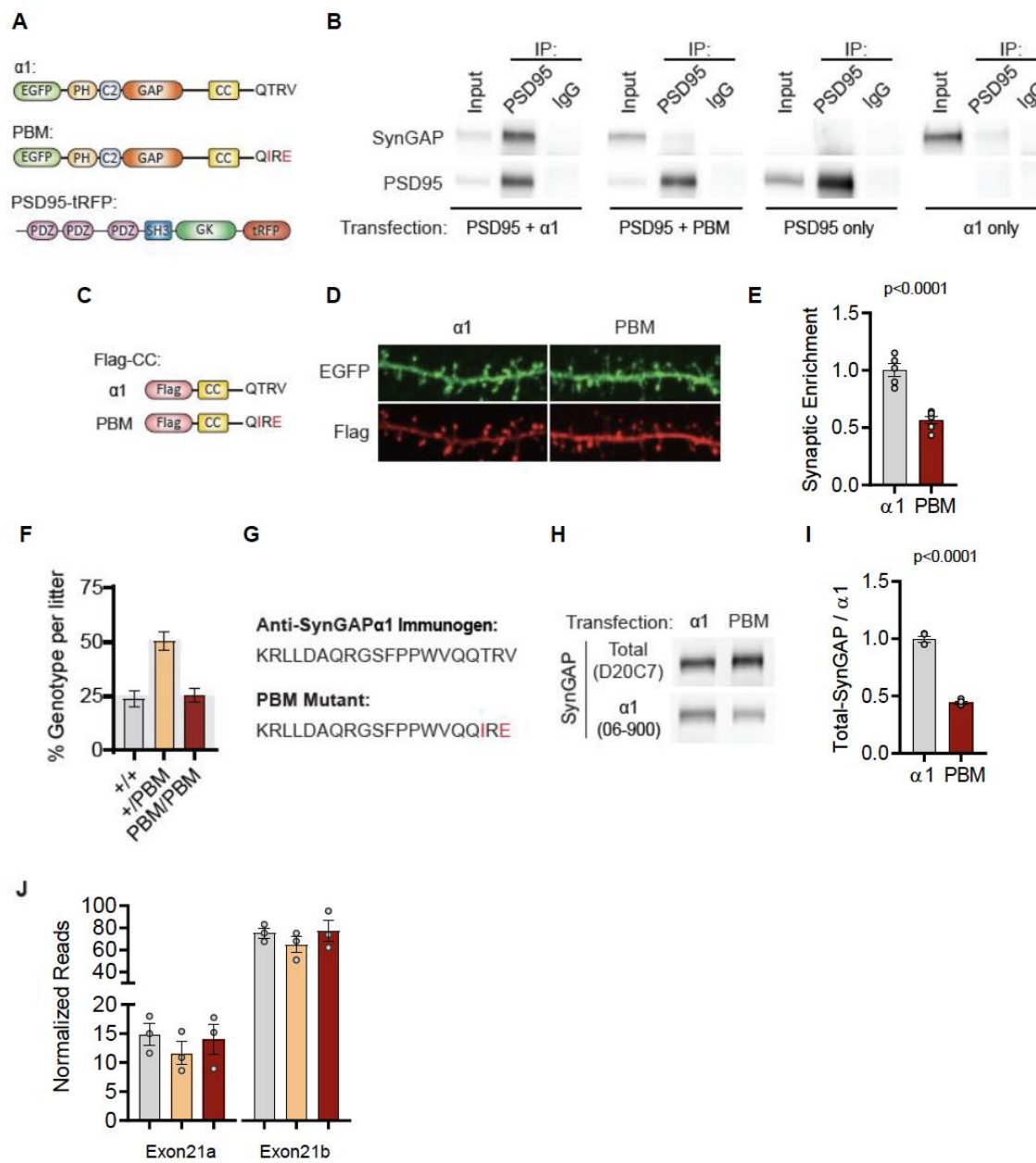
**Total:** (-) allele F(1, 44)=58.57, p<0.0001;  $\beta^*$  allele F(1, 44)=0.1181, p=0.7327. Allelic Interaction F(1, 244)=0.1839, p=0.6701. **α1:** (-) allele F(1, 44)=35.37, p<0.0001;  $\beta^*$  allele F(1, 44)=4.932, p=0.031; Allelic Interaction F(1, 44)=0.3615, p=0.5508. **α2:** (-) allele F(1, 44)=63.95, p<0.0001;  $\beta^*$  allele F(1, 44)=18.00, p<0.0001; Allelic Interaction F(1, 44)=0.03486, p=0.8527. **β:** (-) allele F(1, 20)=9.149, p=0.0067;  $\beta^*$  allele F(1, 20)=9.676, p=0.0055; Allelic Interaction F(1, 20)=0.3027, p=0.5883.



1052  
1053  
1054  
1055  
1056  
1057

**Figure 5 – Validation of SynGAP PDZ binding motif (PBM) mutations and construction of the *Syngap1*<sup>PBM</sup> mouse line. (A)** Schematic diagram for exon map and alternative use of Exon21 in *Syngap1* gene. Exon21b encodes for α1 isoform. Exon 21a encodes for α2 isoform. Point mutations indicated in red alter exon 21b coding sequence without influencing exon21a open reading frame. **(B)** Schematics of SynGAPα1 and PSD95 domain structure and the

1058 location of point mutations. **(C)** Illustrations of constructs expressed in HeLa cells to study PDZ-  
1059 dependent interaction between SynGAP and PSD95. EGFP-CC constructs are homologous to  
1060 SynGAP $\alpha$ 1 C-terminus. **(D)** Co-localization of EGFP-CC $\alpha$ 1 and PSD95-tRFP in HeLa Cells.  
1061 Representative images showing subcellular localizations of WT or PDZ-binding mutant (PBM)  
1062 EGFP-CC $\alpha$ 1 and PSD95-tRFP in HeLa cells when expressed individually or together. **(E)**  
1063 Quantification of (D). Nuclear localization is calculated as the ratio of EGFP signal colocalized  
1064 with DAPI vs total EGFP intensity in within an individual cell. ANOVA with Tukey's multiple  
1065 comparisons test,  $F(3, 96) = 531.4$ .  $p < 0.0001$  **(F)** Schematics of the targeting strategy. The  
1066 targeting vector was spanning Exon20 & 21. The vector included point mutations in Exon21, a  
1067 neomycin resistance selection cassette flanked by Cre recombination sites and diphtheria toxin  
1068 selection cassette (DTA). **(G)** Southern blot analysis showing the genomic DNA of the tested  
1069 heterozygous mice compared to C57BL/6J wild-type DNA. The AflIII digested DNAs were blotted  
1070 on nylon membrane and hybridized with external 5' probe spanning exon19. **(H)** PCR based  
1071 genotyping strategy. Primers flanking leftover LoxP site yields 61bp product in WT and 120bp  
1072 product in mutated allele. **(I)** Representative western blots showing expression levels of total  
1073 SynGAP and individual isoforms in forebrain lysates. **(J)** Quantification of I. Relative intensity of  
1074 bands normalized to total protein signal. Only  $\alpha$ 1 signal is significantly changed.  
1075 ANOVA with Tukey's multiple comparisons test,  $F(2, 14) = 24.86$ ,  $n=5$ .  
1076  
1077

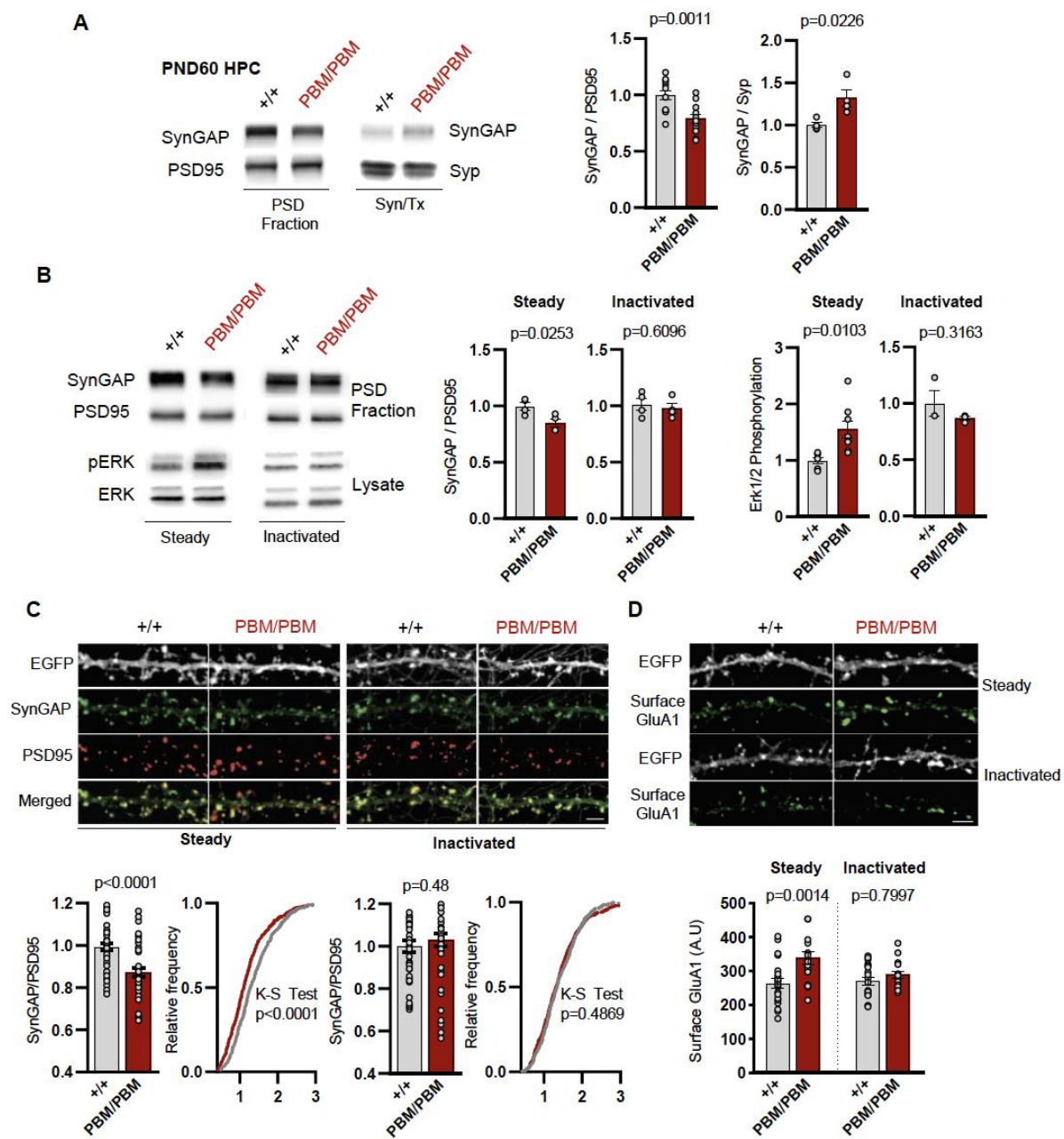


1078  
1079  
1080  
1081  
1082  
1083  
1084  
1085  
1086  
1087  
1088  
1089  
1090  
1091

### Figure 5 - Supplementary

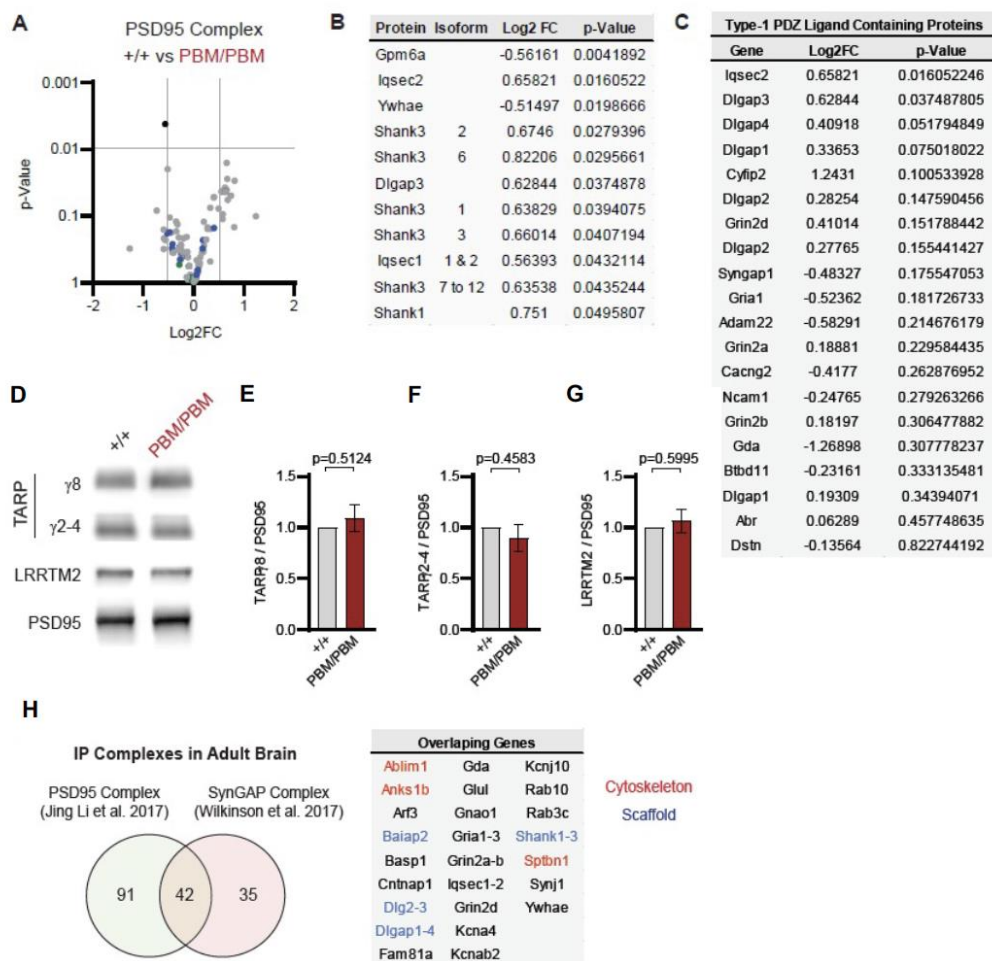
**(A)** Illustrations of constructs expressed in H293T cells to study PDZ-dependent interaction between SynGAP and PSD95. **(B)** Coimmunoprecipitation of PSD-95 and SynGAP $\alpha 1$  from transfected H293T cells. PSD95-tRFP coprecipitates with SynGAP $\alpha 1$ . This Interaction was disrupted by PBM mutations. **(C)** Illustrations of Flag-tagged SynGAP C-terminal constructs expressed in primary cortical neurons. **(D)** Subcellular localization of wild-type or PBM mutated Flag-CC $\alpha 1$  in primary forebrain neurons. Note that Flag-CC $\alpha 1$  is heavily enriched in dendritic spines compared to Flag-CC PBM. Height of the image is 5 $\mu$ m. **(E)** Quantification of synaptic enrichment of Flag-CC constructs. Enrichment in dendritic spines were calculated as the ratio of Flag signal in spines vs dendrites over ratio of EGFP signal in spines vs dendrites. Unpaired t-test,  $t(9)=6.982$   $p < 0.0001$ . Introduced point mutations impeded the enrichment of Flag-tagged SynGAP $\alpha 1$  C-terminal construct in primary forebrain neurons. **(F)** Genotype frequencies observed from 15 litters following heterozygous crosses. Expected mendelian ratio is

1092 highlighted with gray. **(G)** Antigen for  $\alpha 1$ -specific antibody in comparison to PBM mutant C-tail.  
1093 **(H)** Reduced antigenicity of  $\alpha 1$  antibody against PBM mutant C-terminus. H293T cells were  
1094 transfected with either wild-type or PDZ-binding mutant form of EGFP-SynGAP $\alpha 1$ . Lysates were  
1095 probed for both Pan-SynGAP (D20C7) and  $\alpha 1$ -specific (06-800) antibody. Relative reduction in  
1096  $\alpha 1$  to Pan-SynGAP signal demonstrates ~50% reduction in antigenicity. **(I)** Quantification of (D)  
1097 Unpaired t-test.  $t(6)=19.16$ ,  $n=4$ ,  $p<0.0001$ . **(J)** SynGAP  $\alpha 1$  mRNA levels in forebrain  
1098 transcriptome. Normalized reads of Exon21b (specific to  $\alpha 1$ ) were shown in linear scale.  
1099 ANOVA  $F(2,6)=0.3009$ ,  $n=3$ ,  $p=0.7507$ . No significant changes were found across genotypes  
1100 indicating that point mutations do not influence the mRNA expression levels.  
1101  
1102



1103  
1104 **Figure 6 – SynGAP synapse localization in *Syngap1<sup>PBM</sup>* mouse line.** (A) Western blots  
1105 showing relative distribution of SynGAP in PSD and Syn/Tx fractions from adult hippocampi.  
1106 Quantification of western blots probing total SynGAP, Synaptophysin and PSD95. For PSD  
1107 fractions PSD95 and for Syn/Tx fractions Synaptophysin (Syp) were used as loading control.  
1108 PSD fractions:  $t(22)=3.733$ ,  $p=0.0011$   $n=12$  (3 technical replicates for each sample), Syn/TX  
1109 fractions:  $t(6)=3.049$ ,  $p=0.0226$ ,  $n=4$ . Each sample represents hippocampi pooled from 2 mice.  
1110 (B) Western blots showing relative enrichment of (i) SynGAP and PSD95 in PSD fractions  
1111 isolated from DIV18-21 cultures, (ii) phospho and total-ERK1/2 levels in whole cell lysates in  
1112 steady or inactivated state. Synaptic enrichment of SynGAP in (i) steady-state: Unpaired t-test,  
1113  $t(12)=3.040$   $p=0.0103$ . (ii) inactivated state: Unpaired t-test,  $t(6)=0.5385$   $p=0.6096$ . Erk1/2  
1114 phosphorylation is calculated as ratio of phospho- Erk1/2 to total-Erk1/2 in homogenates. Erk1/2  
1115 phosphorylation in (i) steady-state: Unpaired t-test,  $t(6)=2.961$   $p=0.0253$ . (ii) inactivated state:

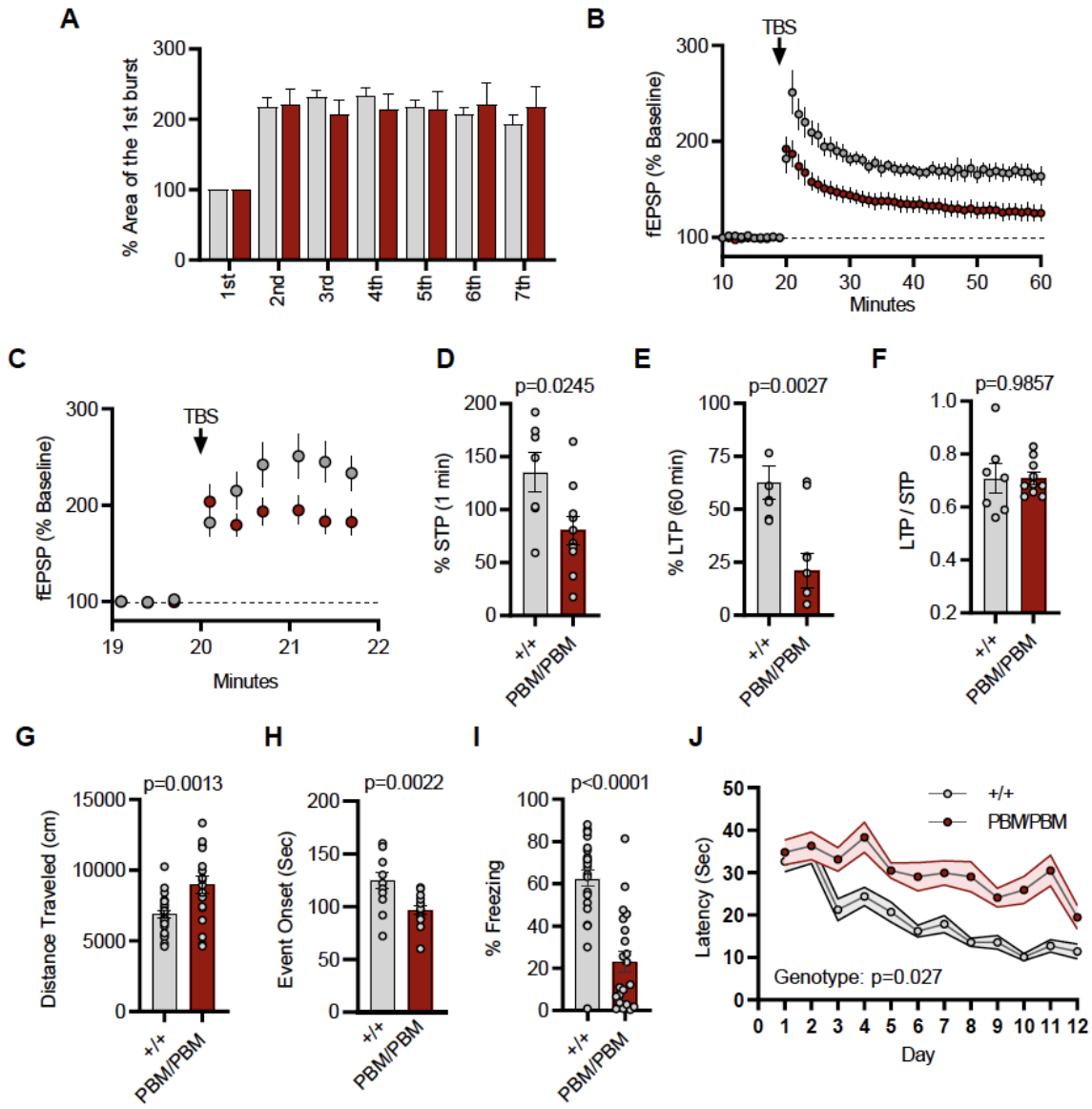
1116 Unpaired t-test,  $t(4)=1.144$   $p=0.3163$  **(C)** Synaptic enrichment of total SynGAP in WT and PBM  
1117 mutants in steady or inactivated state. Levels of SynGAP relative to PSD95 signal in dendritic  
1118 spines. Left, bar graphs demonstrate mean enrichment in an individual dendritic segment.  
1119 Steady-state:  $t(90)=4.393$   $p<0.0001$ . Inactivated:  $t(78)=0.6982$   $p=0.48$ . Cumulative distribution  
1120 of SynGAP to PSD95 ratios in individual synapses. Kolmogorov-Smirnov test, Steady-state:  
1121  $p<0.0001$ , Inactivated:  $p=0.4869$ . **(D)** Surface GluA1 expression in primary forebrain cultures in  
1122 steady or inactivated state. Quantification of mean surface GluA1 levels coincident with PSD95  
1123 puncta. Two-way ANOVA with Tukey's multiple comparisons test. Interaction:  $F(1,74)=4.112$ ,  
1124  $p=0.0462$ , Genotype:  $F(1,74)=11.09$ ,  $p=0.0014$ . Treatment:  $F(1,74)=2.329$ ,  $p=0.1313$ . Each n  
1125 represents an average of 25-30 spines from a dendritic segment belonging to distinct neurons.  
1126  
1127



1128  
1129

1130 **Figure 7 – Characterization of native PSD95 complexes from *Syngap1<sup>PBM</sup>* animals. (A)**  
1131 Volcano plot demonstrating the label-free quantitative mass-spectrometry profile of the  
1132 logarithmic difference in protein levels in the immunoprecipitated PSD95 complexes derived  
1133 from DIV21 +/+ and PBM/PBM cultures in inactivated state. Only Gpm6a (shown in black) was  
1134 significantly altered beyond  $p>0.001$  cutoff. Blue dots represent proteins with type 1 PDZ-  
1135 ligands. Green dots represent DLG family proteins. P values were calculated via t-test for each  
1136 protein. Samples were derived from individual cultures (4 per genotype) which are  
1137 immunoprecipitated separately. Log2FC was calculated as ratio of PBM/PBM over +/+. (B) List  
1138 of proteins that are differentially expressed beyond  $p>0.05$  cutoff. Note that Iqsec2 and Dlgap3  
1139 are PDZ-binding proteins. (C) Mass-spectrometry profile of type-1 PDZ binding motif containing  
1140 proteins in immunoprecipitated PSD95 complex in +/+ vs PBM/PBM inactivated cultures. (D)  
1141 Western blots showing relative expression of TARPs and Lrrtm2 in PSD fractions from adult  
1142 hippocampi in +/+ vs PBM/PBM. (E-G) Quantifications of (D). (E) TARPg8 t(6)=0.6961,  
1143 p=0.5124. (F) TARPg2-4 t(6)=0.7924, p=0.4583 (G) Lrrtm2 t(6)=0.5542, p=0.5995. Each  
1144 sample represents hippocampi pooled from 2 mice. (H) Comparison of PSD95 and SynGAP IP  
1145 complexes as reported by (Li et al. 2017 and Wilkinson et al. 2017). Note that PSD95 and  
1146 SynGAP complexes share diverse range of components involving cytoskeletal and scaffolding  
1147 proteins.

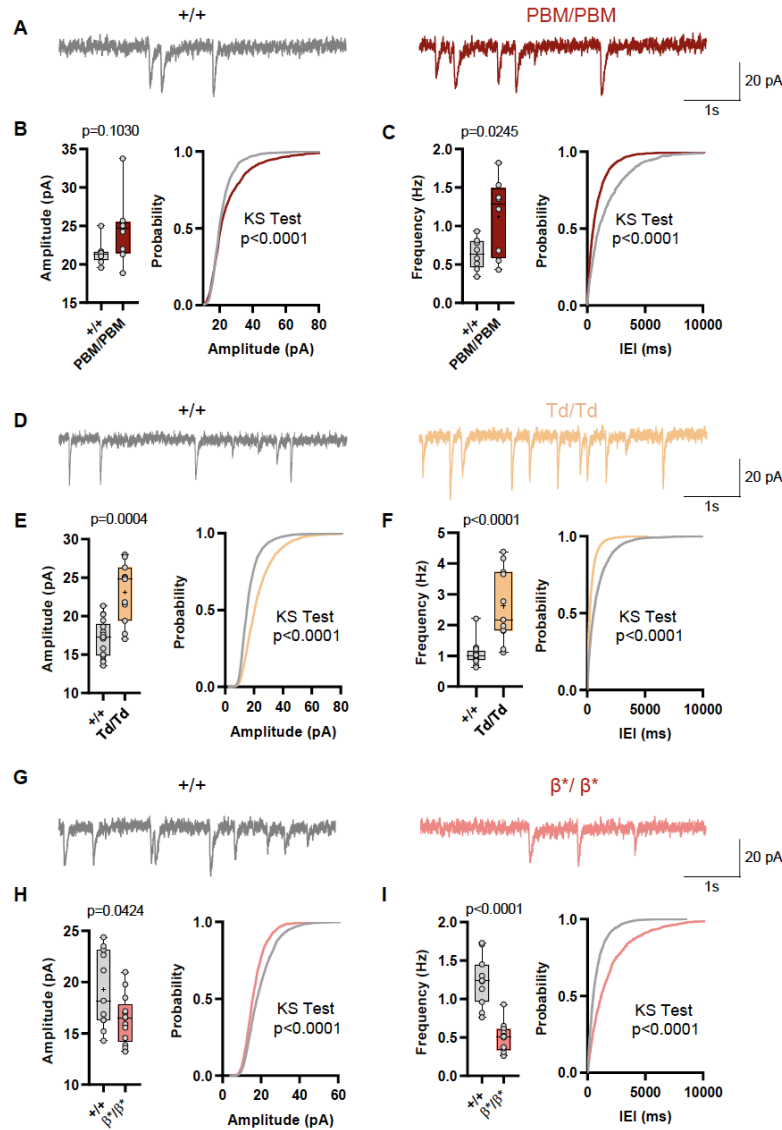
1148  
1149



1150  
1151

1152 **Figure 8 – Plasticity and behavior deficits in the *Syngap1PBM* mouse line. (A)** Facilitation of  
1153 burst responses was calculated by expressing the area of the composite fEPSP corresponding  
1154 to the 2nd theta burst within each train as a fraction of the 1st burst response. No statistically  
1155 significant difference was found between genotypes. **(B)** Magnitude of long-term potentiation  
1156 (LTP) following delivery of a single train of five theta bursts. The slope of the fEPSP was  
1157 normalized to the mean value for a 20 min baseline period; shown are group means and  
1158 standard errors. The control path, to the same site at which LTP was recorded, received 3/min  
1159 pulses throughout the session. **(C)** Percent fEPSP during and immediately after the LTP  
1160 induction. Note that homozygous mutants reach to peak potential immediately following TBS.  
1161 **(D)** Bar graph shows % potentiation in 1 min after stimulus.  $t(15)=2.499$ ,  $p=0.0245$  **(E)** Bar graph  
1162 shows % potentiation in 60 min after stimulus.  $t(15)=3.594$ ,  $p=0.0027$  **(F)** LTP to STP ratio of  
1163 individual slices. Note that the level of LTP is proportional to the degree of acute potentiation  
1164 (1min after stimulus).  $t(15)=0.01818$ ,  $p=0.9857$ . **(G)** Quantification of total distance traveled in  
1165 OFT.  $t(45)=3.427$ ,  $p=0.0013$ . **(H)** Seizure threshold was measured as the time taken to reach  
1166 three separate events of 1st clonus (event onset) during the procedure. Unpaired t-test

1167 t(25)=3.420 p=0.0022. **(I)** Percent freezing in remote contextual fear memory paradigm. %  
1168 Freezing: t(45)=6.463, p<0.0001. **(J)** Plots demonstrating latency to find platform across days in  
1169 Morris Water Maze training session. Statistical significance was determined by using linear  
1170 mixed model for repeated measures. n=14, +/+ vs PBM/PBM, p=0.027  
1171  
1172



1173  
1174

1175 **Figure 9 – Analysis of excitatory synapse function in  $Syngap1^{PBM}$ ,  $Syngap1^{\beta^*}$ , and**  
1176  **$Syngap1^{td}$  mouse lines. (A)** Representative mEPSCs traces from L2/3 SSC in  $+/+$  vs  
1177 PBM/PBM **(B)** Scatter plots and cumulative histograms showing trend towards increase but no  
1178 significant difference in Amplitudes of mEPSCs  $+/+$  vs PBM/PBM **(C)** Scatter plots and  
1179 cumulative histograms showing significant increase in frequency of mEPSCs  $+/+$  vs PBM/PBM.  
1180 Unpaired t test:  $p=0.0245$ ,  $n=8$  for each genotype. **(D)** Representative mEPSCs traces from  
1181 L2/3 SSC in  $+/+$  vs Td/Td. **(E)** Scatter plots and cumulative histograms showing significantly  
1182 increased amplitudes of mEPSCs in  $+/+$  vs Td/Td. Unpaired t test:  $p=0.0004$ ,  $n=17$  cells for  $+/+$ ,  
1183  $n=11$  cells for Td/Td mice. **(F)** Scatter plots and cumulative histograms showing significant  
1184 increase in frequency of mEPSCs in  $+/+$  vs Td/Td. Unpaired t test:  $p<0.0001$ ,  $n=17$  cells for  $+/+$ ,  
1185  $n=11$  cells for Td/Td mice. **(G)** Representative mEPSCs traces from L2/3 SSC in  $+/+$  vs  $\beta^*/\beta^*$ .  
1186 **(H)** Scatter plots and cumulative histograms showing significantly decreased amplitudes of  
1187 mEPSCs in L2/3 SSC for  $+/+$  vs  $\beta^*/\beta^*$ . Unpaired t test:  $p=0.0424$ ,  $n=11$  cells for  $+/+$ ,  $n=13$  cells  
1188 for  $\beta^*/\beta^*$ . **(I)** Scatter plots and cumulative histograms showing significant decrease in frequency  
1189 of mEPSCs in  $+/+$  vs  $\beta^*/\beta^*$ . Unpaired t test:  $p<0.0001$ ,  $n=11$  cells for  $+/+$ ,  $n=13$  cells for  $\beta^*/\beta^*$ .

1190

1191 **References**

1192  
1193

- 1194 1. Deciphering Developmental Disorders, S., *Large-scale discovery of novel genetic*  
1195 *causes of developmental disorders*. *Nature*, 2015. **519**(7542): p. 223-8.
- 1196 2. Deciphering Developmental Disorders, S., *Prevalence and architecture of de novo*  
1197 *mutations in developmental disorders*. *Nature*, 2017. **542**(7642): p. 433-438.
- 1198 3. Hamdan, F.F., et al., *Mutations in SYNGAP1 in autosomal nonsyndromic mental*  
1199 *retardation*. *N Engl J Med*, 2009. **360**(6): p. 599-605.
- 1200 4. Vlaskamp, D.R.M., et al., *SYNGAP1 encephalopathy: A distinctive generalized*  
1201 *developmental and epileptic encephalopathy*. *Neurology*, 2019. **92**(2): p. e96-e107.
- 1202 5. Parker, M.J., et al., *De novo, heterozygous, loss-of-function mutations in SYNGAP1*  
1203 *cause a syndromic form of intellectual disability*. *Am J Med Genet A*, 2015. **167a**(10): p.  
1204 2231-7.
- 1205 6. Mignot, C., et al., *Genetic and neurodevelopmental spectrum of SYNGAP1-associated*  
1206 *intellectual disability and epilepsy*. *J Med Genet*, 2016. **53**(8): p. 511-22.
- 1207 7. Iossifov, I., et al., *The contribution of de novo coding mutations to autism spectrum*  
1208 *disorder*. *Nature*, 2014. **515**(7526): p. 216-21.
- 1209 8. Satterstrom, F.K., et al., *Large-Scale Exome Sequencing Study Implicates Both*  
1210 *Developmental and Functional Changes in the Neurobiology of Autism*. *Cell*, 2020.  
1211 **180**(3): p. 568-584 e23.
- 1212 9. Holder, J.L., Jr., F.F. Hamdan, and J.L. Michaud, *SYNGAP1-Related Intellectual*  
1213 *Disability*, in *GeneReviews((R))*, M.P. Adam, et al., Editors. 1993: Seattle (WA).
- 1214 10. Weldon, M., et al., *The first international conference on SYNGAP1-related brain*  
1215 *disorders: a stakeholder meeting of families, researchers, clinicians, and regulators*. *J*  
1216 *Neurodev Disord*, 2018. **10**(1): p. 6.
- 1217 11. Llamosas, N., et al., *SYNGAP1 Controls the Maturation of Dendrites, Synaptic Function,*  
1218 *and Network Activity in Developing Human Neurons*. *J Neurosci*, 2020. **40**(41): p. 7980-  
1219 7994.
- 1220 12. Kilinc, M., et al., *Species-conserved SYNGAP1 phenotypes associated with*  
1221 *neurodevelopmental disorders*. *Molecular and Cellular Neuroscience*, 2018. **91**: p. 140-  
1222 150.
- 1223 13. Gamache, T.R., Y. Araki, and R.L. Huganir, *Twenty Years of SynGAP Research: From*  
1224 *Synapses to Cognition*. *J Neurosci*, 2020. **40**(8): p. 1596-1605.
- 1225 14. Kim, J.H., et al., *SynGAP: a synaptic RasGAP that associates with the PSD-95/SAP90*  
1226 *protein family*. *Neuron*, 1998. **20**(4): p. 683-91.
- 1227 15. Chen, H.J., et al., *A synaptic Ras-GTPase activating protein (p135 SynGAP) inhibited by*  
1228 *CaM kinase II*. *Neuron*, 1998. **20**(5): p. 895-904.
- 1229 16. Ozkan, E.D., et al., *Reduced cognition in Syngap1 mutants is caused by isolated*  
1230 *damage within developing forebrain excitatory neurons*. *Neuron*, 2014. **82**(6): p. 1317-  
1231 33.
- 1232 17. Araki, Y., et al., *Rapid dispersion of SynGAP from synaptic spines triggers AMPA*  
1233 *receptor insertion and spine enlargement during LTP*. *Neuron*, 2015. **85**(1): p. 173-89.
- 1234 18. Clement, J.P., et al., *Pathogenic SYNGAP1 mutations impair cognitive development by*  
1235 *disrupting maturation of dendritic spine synapses*. *Cell*, 2012. **151**(4): p. 709-23.
- 1236 19. Clement, J.P., et al., *SYNGAP1 links the maturation rate of excitatory synapses to the*  
1237 *duration of critical-period synaptic plasticity*. *J Neurosci*, 2013. **33**(25): p. 10447-52.
- 1238 20. Aceti, M., et al., *Syngap1 Haploinsufficiency Damages a Postnatal Critical period of*  
1239 *Pyramidal Cell Structural Maturation Linked to Cortical Circuit Assembly*. *Biological*  
1240 *Psychiatry*, 2015.

1241 21. Michaelson, S.D., et al., *SYNGAP1 heterozygosity disrupts sensory processing by*  
1242 *reducing touch-related activity within somatosensory cortex circuits*. *Nature*  
1243 *Neuroscience*, 2018. **21**(12): p. 1-13.

1244 22. Araki, Y., et al., *SynGAP isoforms differentially regulate synaptic plasticity and dendritic*  
1245 *development*. *Elife*, 2020. **9**.

1246 23. Gou, G., et al., *SynGAP splice variants display heterogeneous spatio-temporal*  
1247 *expression and subcellular distribution in the developing mammalian brain*. *J*  
1248 *Neurochem*, 2020. **154**(6): p. 618-634.

1249 24. McMahon, A.C., et al., *SynGAP isoforms exert opposing effects on synaptic strength*.  
1250 *Nat Commun*, 2012. **3**: p. 900.

1251 25. Rumbaugh, G., et al., *SynGAP regulates synaptic strength and mitogen-activated*  
1252 *protein kinases in cultured neurons*. *Proceedings of the National Academy of Sciences*  
1253 *of the United States of America*, 2006. **103**(12): p. 4344-4351.

1254 26. Vazquez, L.E., et al., *SynGAP regulates spine formation*. *J Neurosci*, 2004. **24**(40): p.  
1255 8862-72.

1256 27. Komiya, N.H., et al., *SynGAP regulates ERK/MAPK signaling, synaptic plasticity, and*  
1257 *learning in the complex with postsynaptic density 95 and NMDA receptor*. *J Neurosci*,  
1258 2002. **22**(22): p. 9721-32.

1259 28. Sullivan, B.J., et al., *Low-Dose Perampanel Rescues Cortical Gamma Dysregulation*  
1260 *Associated With Parvalbumin Interneuron GluA2 Upregulation in Epileptic Syngap1(+-)*  
1261 *Mice*. *Biol Psychiatry*, 2020. **87**(9): p. 829-842.

1262 29. Spicer, T.P., et al., *Improved Scalability of Neuron-Based Phenotypic Screening Assays*  
1263 *for Therapeutic Discovery in Neuropsychiatric Disorders*. *Mol Neuropsychiatry*, 2018.  
1264 **3**(3): p. 141-150.

1265 30. Kim, J.H., et al., *The role of synaptic GTPase-activating protein in neuronal development*  
1266 *and synaptic plasticity*. *J Neurosci*, 2003. **23**(4): p. 1119-24.

1267 31. Yokoi, S., et al., *3'UTR Length-Dependent Control of SynGAP Isoform alpha2 mRNA by*  
1268 *FUS and ELAV-like Proteins Promotes Dendritic Spine Maturation and Cognitive*  
1269 *Function*. *Cell Rep*, 2017. **20**(13): p. 3071-3084.

1270 32. Creson, T.K., et al., *Re-expression of SynGAP protein in adulthood improves*  
1271 *translatable measures of brain function and behavior*. *eLife*, 2019. **8**: p. e46752.

1272 33. Guo, X., et al., *Reduced expression of the NMDA receptor-interacting protein SynGAP*  
1273 *causes behavioral abnormalities that model symptoms of Schizophrenia*.  
1274 *Neuropsychopharmacology*, 2009. **34**(7): p. 1659-72.

1275 34. Zeng, M., et al., *Phase Transition in Postsynaptic Densities Underlies Formation of*  
1276 *Synaptic Complexes and Synaptic Plasticity*. *Cell*, 2016. **166**(5): p. 1163-1175.e12.

1277 35. Gou, G., et al., *SynGAP Splice Variants Display Heterogeneous Spatio-Temporal*  
1278 *Expression And Subcellular Distribution In The Developing Mammalian Brain*. *bioRxiv*,  
1279 2019: p. 681148.

1280 36. Li, J., et al., *Spatiotemporal profile of postsynaptic interactomes integrates components*  
1281 *of complex brain disorders*. *Nature Neuroscience*, 2017. **20**: p. 1150.

1282 37. Wilkinson, B., J. Li, and M.P. Coba, *Synaptic GAP and GEF Complexes Cluster Proteins*  
1283 *Essential for GTP Signaling*. *Scientific Reports*, 2017. **7**(1): p. 5272.

1284 38. Volianskis, A., et al., *Different NMDA receptor subtypes mediate induction of long-term*  
1285 *potentiation and two forms of short-term potentiation at CA1 synapses in rat*  
1286 *hippocampus in vitro*. *The Journal of Physiology*, 2013. **591**(4): p. 955-972.

1287 39. Wang, C.-C., R.G. Held, and B.J. Hall, *SynGAP Regulates Protein Synthesis and*  
1288 *Homeostatic Synaptic Plasticity in Developing Cortical Networks*. *PLoS ONE*, 2013.  
1289 **8**(12): p. e83941.

1290 40. Hamdan, F.F., et al., *De novo SYNGAP1 mutations in nonsyndromic intellectual*  
1291 *disability and autism*. *Biol Psychiatry*, 2011. **69**(9): p. 898-901.

1292 41. Berryer, M.H., et al., *Mutations in SYNGAP1 cause intellectual disability, autism, and a*  
1293 *specific form of epilepsy by inducing haploinsufficiency*. *Hum Mutat*, 2013. **34**(2): p. 385-  
1294 94.

1295 42. Lim, K.H., et al., *Antisense oligonucleotide modulation of non-productive alternative*  
1296 *splicing upregulates gene expression*. *Nat Commun*, 2020. **11**(1): p. 3501.

1297 43. Zhang, L.I. and M.M. Poo, *Electrical activity and development of neural circuits*. *Nature*  
1298 *Neuroscience*, 2001. **4**: p. 1207-1214.

1299 44. Lynch, G., C.S. Rex, and C.M. Gall, *LTP consolidation: substrates, explanatory power,*  
1300 *and functional significance*. *Neuropharmacology*, 2007. **52**(1): p. 12-23.

1301 45. Dravid, S.M., et al., *Subunit-specific mechanisms and proton sensitivity of NMDA*  
1302 *receptor channel block*. *J Physiol*, 2007. **581**(Pt 1): p. 107-28.

1303